Assessment of aerosol iron (Fe) solubility using global dataset, Part I: Mechanisms underlying the inverse relationship between Fe solubility and Fe concentration

Kohei Sakata[1], Minako Kurisu[2], Yoshio Takahashi[3]

[1]Materials Science and Engineering, Graduate School of Engineering, Tokyo Denki University, 5 Senjyu-Asahi-Cho, Adachi-ku, Tokyo 120-8551, Japan.

[2]Atmosphere and Ocean Research Institute, The University of Tokyo, 5-1-5, Kashiwanoha, Kashiwa, Chiba 277-8564, Japan.

[3]Graduate School of Science, The University of Tokyo, 7-3-1, Hongo Bunkyo-ku, Tokyo 113-0033, Japan.

Corresponding author: Kohei Sakata (kohei.sakata.33@mail.dendai.ac.jp)

ORCID: 0000-0002-0103-9631

Abstract.

Atmospheric deposition of aerosol iron (Fe) can stimulate marine primary productivity by supplying dissolved Fe (d-Fe) to the surface ocean, thereby potentially influencing the global climate. Aerosol Fe solubility (Fe_{sol}%) is closely linked to its bioavailability, and previous studies have shown that Fe_{sol}% generally increases as aerosol Fe concentration decreases. However, the mechanism underlying this widely observed inverse relationship remains unresolved. In this study, aerosol observations from East Asia, the North and South Pacific, and the Atlantic were compiled, and the enrichment factor of total Fe ($EF_{T\text{-}Fe}$ = $(T\text{-}Fe/T\text{-}Al)_{aerosol}/(T\text{-}Fe/T\text{-}Al)_{crust}$) and dissolved Fe to dissolved Al ([d-Fe]/[d-Al]) were used to estimate the contributions of mineral-derived and anthropogenic Fe to aerosol d-Fe, as well as the Fe_{sol}% of each source fraction. Aerosol d-Fe was found to be derived predominantly from mineral dust in many oceanic regions. In addition, both mineral-derived Fe and anthropogenic Fe showed inverse relationships between concentration and solubility. If the inverse relationship between Fe concentration and Fe_{sol}% were controlled mainly by simple two-component mixing between low-solubility mineral particles and highly soluble anthropogenic Fe, the Fe_{sol}% of each source fraction would not be expected to vary systematically with concentration. Instead, the results suggest that atmospheric chemical processing, together with depositional removal during transport, progressively increases the solubility of Fe remaining in aerosol particles. The ability to estimate the sources and dissolution processes of aerosol Fe from such fundamental concentration data may help improve the parameterization of aerosol Fe dissolution in global climate models.

1 Introduction

Aerosol particles play a central role in the biogeochemical cycling of the Earth's surface environment. One key process is the fertilization of the oceans by aerosol-derived iron (Fe) (Jickells et al., 2005; Mahowald et al., 2009; Kanakidou et al., 2018). In high-nutrient, low-chlorophyll (HNLC) regions, primary production is limited by the scarcity of dissolved iron (d-Fe) in surface waters (Martin and Fitzwater, 1988; Martin, 1990; Martin et al., 1994; Boyd et al., 2007). The addition of d-Fe to these regions stimulates the biological pump, thereby influencing the cycling of carbon, nitrogen, sulfur, and Fe (Charlson et al., 1987; Krishnamurthy et al., 2009; Jin et al., 2008). Aerosols are recognized as a major source of d-Fe to the surface ocean, and numerous studies have examined this contribution (Baker et al., 2006a, 2006b, 2013, 2020; Buck et al., 2006, 2010a, 2010b, 2013; Chance et al., 2015; Shelley et al., 2018; Marsay et al., 2022; Sakata et al., 2022; Kurisu et al., 2021, 2024). These studies indicate that the fractional Fe solubility (Fe_{sol}%) in aerosols is primarily governed by (i) differences in Fe_{sol}% among emission sources (e.g., mineral dust, volcanic ash, anthropogenic aerosols) and their relative abundances, and (ii) chemical alterations, including proton-promoted, ligand-promoted, and photoreductive Fe dissolutions. However, the relative importance of these factors of Fe_{sol}% remains poorly constrained (Mahowald et al., 2009, 2018; Olgun et al., 2011; Sholkovitz et al., 2012; Ito et al., 2019; Baker et al., 2021).

Although several recent studies have examined the seasonal variability of Fe_{sol}% (Takahashi et al., 2013; Sakata et al., 2023, 2025; Zhang et al., 2023; Chen et al., 2026), such observations remain scarce globally, contributing to uncertainty in identifying the factors controlling Fe solubility. The supply of aerosol Fe from East Asia to the North Pacific is modulated by seasonal variations in both natural and anthropogenic sources. Mineral dust loading typically peaks in March-May (Uematsu et al., 1983; Zhu et al., 2020; Kawai et al., 2021), whereas concentrations of several anthropogenic pollutants increase in December-February due to higher residential fuel combustion (Ma et al., 2017; Zhang et al., 2018; Kurokawa and Ohara, 2020). Previous work suggests that anthropogenic Fe (anthro-Fe) generally exhibits higher Fe_{sol}% than mineral dust, implying that seasonal changes in their relative contributions influence Fe_{sol}% overall. Aerosol pH, which controls Fe dissolution rates, particularly for proton-promoted processes, also varies seasonally in response to temperature and humidity changes (Guo et al., 2016; Tao and Murphy, 2019a; Song and Osada, 2020; Pye et al., 2020; Zheng et al., 2020). Consequently, Fe_{sol}% is also expected to exhibit seasonal variability. Given that most Fe in marine aerosols originates from continental regions, long-term observations in both marine and continental atmospheres are essential for identifying the controlling factors of Fe_{sol}%. However, studies covering longer than one year are scarce, even at land-based sites, and conducting such long-term observations during research cruises is particularly challenging. Moreover, only limited attempts have been made to compile existing measurement data to systematically evaluate the seasonal variability of Fe_{sol}% and the mechanisms governing it in marine aerosols.

To understand the seasonal variability of Fe_{sol}% in aerosols collected from both terrestrial and marine atmospheres, as well as to elucidate the controlling factors, it is essential to compile existing data and discuss them in detail. This study compiled a global dataset from previous observational work and associated measurements of total and dissolved Fe and Al concentrations and their solubilities. The dataset encompasses East Asia (Duvall et al., 2008; Li et al., 2015; Kurisu et al.,

2019; Hsieh et al., 2023; Sakata et al., 2023, 2025; Seo and Kim, 2023), the North Pacific (Buck et al., 2006, 2013; Marsay et al., 2022; Sakata et al., 2022; Kurisu et al., 2024), the South Pacific (Buck et al., 2013, 2019; Sakata et al., 2022; Perron et al., 2020a, 2021), and the Atlantic Ocean (Baker et al., 2006a, 2006b, 2013, 2020; Buck et al., 2010a, 2010b; Chance et al., 2015). We included Al data because a plot of the enrichment factor of total Fe ($EF_{T\text{-}Fe}$ = $(T\text{-}Fe/T\text{-}Al)_{aerosol}/(T\text{-}Fe/T\text{-}Al)_{crust}$) plotted against the molar concentration ratio of d-Fe to dissolved Al ([d-Fe]/[d-Al]) is a useful tool for identifying emission sources of T-Fe and d-Fe (Sakata et al., 2023). We first calculated monthly means of T-Fe and T-Al concentrations and solubilities to characterize seasonal variabilities. We then estimated the contribution of anthropogenic-derived d-Fe to total aerosol d-Fe, and separately evaluated the Fe_{sol}% of mineral dust and anthropogenic aerosols to assess the seasonal variability of their atmospheric alteration processes. Finally, we reanalyzed the compiled data using standardized metrics, including $EF_{T\text{-}Fe}$ and [d-Fe]/[d-Al], to investigate the factors controlling Fe_{sol}%. This reanalysis aimed both to clarify spatiotemporal patterns linked to these controlling factors and to identify key gaps that should be addressed in future observational studies.

2 Methods

2.1 Data compilation of total and dissolved Fe and Al concentrations

This study primarily utilized data reported in previous observations, supplemented by our unpublished data from size-resolved aerosol samples collected in the Pacific Ocean. Detailed descriptions of the sampling and analytical procedures for these unpublished data are provided in Section S1 of the Supplementary Information. For data compilation, only samples for which concentrations of T-Fe, T-Al, d-Fe, and d-Al were concurrently available were included. In certain studies, d-Fe and d-Al concentrations were derived based on their corresponding Fe_{sol}% or Al_{sol}%. All compiled data were acquired through filter-based collection methods. Aerosol particles were sampled using cellulose, quartz fiber, or PTFE fiber filters (Buck and Paytan, 2012; Morton et al., 2013; Sakata et al., 2018). While the majority of previous studies collected total suspended particulates (TSP), size-fractionated aerosol samples were occasionally utilized. In this study, coarse and fine aerosol particles are defined as those with aerodynamic diameters greater than or less than 2.5 μm, respectively. Samples were predominantly preserved by freezing at –20°C or by storage in a desiccator at ambient temperature under dry conditions (approximately 20% relative humidity).

Given the variability in acid digestion and extraction protocols for Fe and Al across studies, specific criteria were established for data compilation. A critical consideration was whether hydrofluoric acid (HF) was incorporated in the digestion process. It is known that the incomplete digestion of Si-O bonds present in aluminosilicates, due to the omission of HF, leads to an underestimation of the T-Fe and T-Al concentrations that are substituted or trapped within the minerals (Chao and Sanzolne, 1992; Mitra and Rimstidt, 2009). Therefore, in this study, we only compiled concentrations obtained from aerosol samples digested with acids that included both HNO_3 and HF, following the methodology of Morton et al. (2013). These

elemental concentrations were primarily determined by inductively coupled plasma mass spectrometry (ICP-MS) or inductively coupled plasma optical emission spectroscopy (ICP-OES), with occasional utilization of X-ray fluorescence analysis (XRF) in the absence of total acid digestion.

Extraction solutions (e.g., ultrapure water, weak or strong ligand solutions), extraction methodologies (batch versus flow-through), and extraction durations varied among the referenced studies (Sholkovitz et al., 2012; Baker and Croot, 2010; Clough et al., 2020; Perron et al., 2020b). In this study, Fe extracted by ultrapure water and ammonium acetate buffer were uniformly classified as d-Fe, with the same approach applied for Al. Most aerosol samples from East Asia and the Pacific were extracted using ultrapure water, whereas a subset of Atlantic samples underwent extraction using ammonium acetate buffer at pH 4.7.

2.2 Enrichment factor of Fe

To evaluate the sources of T-Fe in aerosol particles (*i.e.*, mineral Fe or anthro-Fe), the enrichment factor of Fe ($EF_{T\text{-}Fe}$) in aerosol particles is calculated by the following equation:

$$EF_{T-Fe} = \frac{(T-Fe/T-Al)_{aerosol}}{(T-Fe/T-Al)_{upper\ continental\ crust}} \qquad \text{(Eq. 1)}$$

where $(T\text{-}Fe/T\text{-}Al)_{aerosol\ or\ upper\ continental\ crust}$ are mass ratio of T-Fe relative to T-Al ratio in aerosol particles and the average upper continental crust (UCC), respectively. Considering that T-Fe/T-Al ratio of the UCC varies among literatures, the $EF_{T\text{-}Fe}$ for all aerosol particles were recalculated. In this study, a mean T-Fe/T-Al ratio of 0.52 ± 0.12, derived from five reported values for the upper continental crust, was used as the reference value to account for variability in crustal T-Fe/T-Al ratios (Turekian, 1961; Taylor, 1964; Taylor and McLennan, 1995; Wedepohl, 1995; Rudnick and Gao, 2003). $EF_{T\text{-}Fe}$ values exceeding 10 are commonly used to indicate a substantial contribution from anthro-Fe. This threshold corresponds to a measured T-Fe/T-Al ratio in aerosol particles exceeding 5.2. In this study, a lower $EF_{T\text{-}Fe}$ threshold of 2.0 was adopted to include samples with possible anthro-Fe contributions; this threshold corresponds to a measured T-Fe/T-Al ratio exceeding 1.04. This decision was made because even after accounting for the T-Fe/T-Al ratio and twice its standard deviation in source samples of Asian dust, Saharan dust, and other mineral dust, a statistically significant difference remained compared to twice the T-Fe/T-Al ratio of upper continental crust (Liu et al., 2022).

2.3 Principle for a diagram between the $EF_{T\text{-}Fe}$ and [d-Fe]/[d-Al] ratio

The [d-Fe]/[d-Al] ratio and $EF_{T\text{-}Fe}$ in aerosol particles vary depending on emission sources and the dissolution processes of aerosol Fe (Sakata et al., 2023). The dominant sources of T-Fe and d-Fe in aerosol particles can be categorized into five groups (Figure 1). $EF_{T\text{-}Fe}$ (vertical axis) is elevated by the influence of T-Fe-rich anthropogenic aerosols, whereas [d-Fe]/[d-Al] (horizontal axis) fluctuates mainly due to mineral dust dissolution processes, including proton-promoted and ligand-promoted dissolutions, and the input of highly soluble anthro-Fe. Aerosol samples strongly influenced by mineral dust are predominantly plotted within areas (i) and (ii), both characterized by $EF_{T\text{-}Fe}$ below 2.0. These areas differ based on the

dissolution mechanisms of mineral dust. Area (i): [d-Fe]/[d-Al] ranging from 0.1 to 1.0 is associated with proton-promoted dissolution (Kodama and Schnitzer, 1973; Desboeufs et al., 2001; Lowson et al., 2005; Duvall et al., 2008; Shi et al., 2011a, Bibi et al., 2015; Bray et al., 2015). Area (ii): [d-Fe]/[d-Al] over 1.0 is associated with ligand-promoted dissolution, for example by oxalate (Kodama and Schnitzer, 1973; Bray et al., 2015). Indeed, [d-Fe]/[d-Al] ratio of Asian dust (0.24 ± 0.20) and Arizona test dust (0.23 ± 0.01) were within the range. Saharan dust has a [d-Fe]/[d-Al] ratio of 0.10 ± 0.04, close to the lower limit of the [d-Fe]/[d-Al] ratio observed for aluminosilicate minerals (Shi et al., 2011a; Desboeufs et al., 2024). Area (ii), where [d-Fe]/[d-Al] exceeds 1.00, is associated with ligand-promoted dissolution, for example by oxalate (Kodama and Schnitzer, 1973; Bray et al., 2015).

Aerosol particles plotted in areas (iii) and (iv) are influenced by anthro-Fe, indicated by $EF_{T\text{-}Fe}$ greater than 2.0, with the distinction between these areas being the solubility of the anthro-Fe. In area (iii), insoluble anthro-Fe is primarily thought to stem from sources like non-exhaust vehicle particles (e.g., brake pad wear) and steel slag, which exhibited high T-Fe/T-Al ratio compared to mineral dust. The Fe_{sol}% of these anthro-Fe (<0.01%) is markedly lower than that of fresh mineral dust (Fe_{sol}%: 0.10–1.00%) (Shupert et al., 2013; Halle et al., 2021; Cui et al., 2025). As a result, although anthro-Fe contributes to enhance T-Fe/T-Al ratio, it has little impact on [d-Fe]/[d-Al] ratio. Therefore, [d-Fe]/[d-Al] ratio of aerosol particles in area (iii) is similar to mineral dust. In contrast, the anthro-Fe in area (iv) is easily dissolved, leading to an increase in the [d-Fe]/[d-Al] ratio. The readily soluble anthro-Fe discussed here includes both initially soluble anthro-Fe with high Fe_{sol}% at emission and initially insoluble anthro-Fe plotted in area (iii), which subsequently becomes more soluble through proton-promoted and ligand-promoted dissolutions. Finally, aerosol particles in area (v) originate from aluminosilicate glasses primarily emitted during combustion processes, including coal burning and municipal solid waste incineration, and are characterized by a [d-Fe]/[d-Al] ratio below 0.10 (Seidel and Zimmels, 1998; Praharaj et al., 2002; Kim et al., 2003; Huang et al., 2007; Chang et al., 2009; Gitari et al., 2009; Komonweeraket et al., 2015)). Additionally, some samples from the Sharan Desert showed values below 0.1, suggesting that these sources may also occasionally contribute (Shi et al., 2011a; Desboeufs et al., 2024).

Assuming a binary mixing between areas (i) and (iv) in Figure 1, the fractions of d-Fe derived from mineral dust ($f_{mineral\text{-}dFe}$) and anthro-Fe ($f_{anthro\text{-}dFe}$) in aerosol particles are estimated by the following equations:

$$f_{mineral-dFe} + f_{anthro-dFe} = 100\% \qquad \text{(Eq.2)}$$

$$\left(\left[\frac{\mathrm{d-Fe}}{\mathrm{d-Al}}\right]\right)_{\mathrm{aerosol}} = \left(\left[\frac{\mathrm{d-Fe}}{\mathrm{d-Al}}\right]\right)_{\mathrm{mineral}} \times f_{mineral-dFe} + \left(\left[\frac{\mathrm{d-Fe}}{\mathrm{d-Al}}\right]\right)_{\mathrm{anthro}} \times f_{anthro-dFe} \qquad \text{(Eq. 3)}$$

A key limitation of this approach is the selection of appropriate representative [d-Fe]/[d-Al] for mineral dust and anthro-Fe. Representative [d-Fe]/[d-Al] ratios of mineral dust in East Asian/North Pacific and Atlantic aerosols were determined utilizing the values derived from Asian dust (= 0.24 ± 0.20, Duvall et al., 2008) and Saharan dust (= 0.11 ± 0.06, Desboeufs et al., 2001, 2024; Shi et al., 2011a). The mean [d-Fe]/[d-Al] ratio of fine aerosol particles collected in East Asia exceeding 1.5 was adopted as the representative [d-Fe]/[d-Al] ratio for anthro-Fe, yielding a value of 2.67 ± 1.88 (Sakata et al., 2023).

Previous studies have reported that Fe_{sol}% and Al_{sol}% obtained by acetate buffer extraction are higher than those obtained by ultrapure water extraction (Clough et al., 2019; Perron et al., 2020b; Tang et al., 2025). However, the increase in Fe_{sol}%

caused by acetate buffer extraction varies widely among studies, ranging from 1.4- to 7.0-fold (Perron et al., 2020b; Tang et al., 2025), making it difficult to apply a consistent correction factor. Therefore, no correction was applied to the solubilities obtained by acetate buffer extraction in this study. In addition, because the ratio of the increases in Fe_{sol}% and Al_{sol}% does not exceed a factor of two (Tang et al., 2025), the effect of extraction method on the [d-Fe]/[d-Al] ratio is expected to be relatively small, and no correction was applied to the [d-Fe]/[d-Al] ratios obtained by acetate buffer extraction. Therefore, the influence of differences in extraction methods on the source apportionment of T-Fe and d-Fe based on this diagram is considered to be limited.

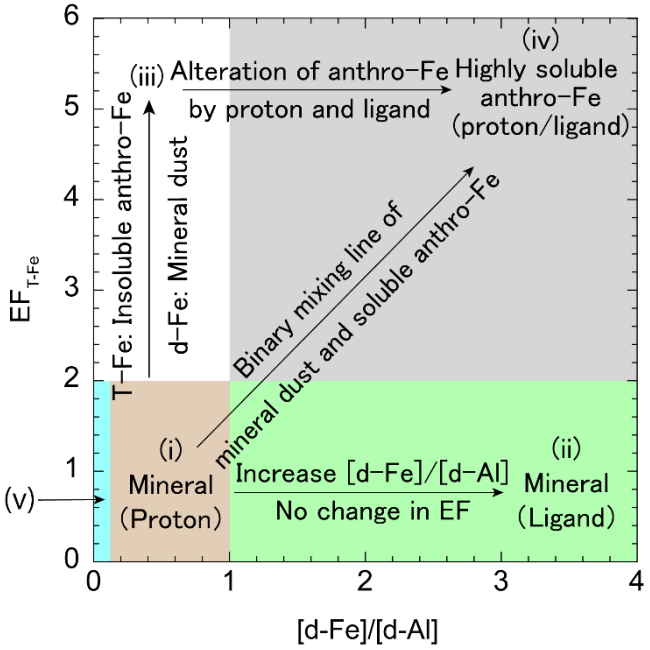

Figure 1. Relationships of emission sources of T-Fe and d-Fe with [d-Fe]/[d-Al] ratio and $EF_{T\text{-}Fe}$. This figure was partially modified from Sakata et al. (2025).

2.4 Calculation of source-specific Fe solubility

The Fe_{sol}% and Al_{sol}% were calculated by the following equations:

$$Fe_{sol}\% = \left(\frac{d-Fe}{T-Fe}\right)_{aerosol} \times 100 \qquad \text{(Eq. 4)}$$

$$Al_{sol}\% = \left(\frac{d-Al}{T-Al}\right)_{aerosol} \times 100 \qquad \text{(Eq. 5)}$$

In this study, Fe_{sol}% of mineral dust and anthropogenic aerosol (mineral-Fe_{sol}% and anthro-Fe_{sol}%, respectively) were evaluated separately. Mineral-Fe and anthro-Fe concentrations were determined using the following equations:

$$\text{Mineral Fe (ng m}^{-3}) = \text{Total Al} \times \left(\frac{T-Fe}{T-Al}\right)_{aerosol} \qquad \text{(Eq. 6)}$$

$$\text{Anthro Fe (ng m}^{-3}) = \text{Total Fe} - \text{Mineral Fe} \quad \text{(Eq. 7)}$$

The d-Fe concentrations dissolved from mineral dust and anthro-Fe (mineral-dFe and anthro-dFe, respectively) were calculated by multiplying the d-Fe concentration by $f_{mineral\text{-}dFe}$ and $f_{anthrod\text{-}Fe}$, respectively.

$$\text{Mineral dFe} = \text{dFe} \times f_{mineral-dFe} \quad \text{(Eq. 8)}$$

$$\text{Anthro dFe} = \text{dFe} \times f_{anthro-dFe} \quad \text{(Eq. 9)}$$

Finally, mineral-Fe_{sol}% and anthro-Fe_{sol}% were calculated using the same equation as Eq. 4.

3. Results and Discussion

3.1 Overview of global dataset

This compiled dataset integrates aerosol samples collected in East Asia with marine aerosol samples observed over the North and South Pacific, and Atlantic for which T-Fe, d-Fe, T-Al, and d-Al concentrations were all available. In total, the dataset includes 1,096 samples (East Asia: 428; North Pacific: 233; South Pacific: 91; Atlantic: 361), comprising TSP from all four regions and size-resolved coarse aerosol particles and fine aerosol particles from East Asia and the North Pacific where such measurements were available. Table 1 summarizes, for TSP in each region and basin, the dominant sources of T-Fe and d-Fe, as well as T-Fe concentration, d-Fe concentration, Fe_{sol}%, and $f_{anthro\text{-}dFe}$. Across the full dataset, T-Fe concentrations ranged from <0.1 to 14166.7 ng m^{-3} (mean: 278.1 ± 860.7 ng m^{-3}; median: 33.3 ng m^{-3}). High-T-Fe samples occurred mainly in East Asia, whereas samples from the North Pacific and South Pacific were concentrated in the low-T-Fe range; Atlantic samples showed an intermediate distribution (Table 1). d-Fe concentrations ranged from <0.1 to 212.7 ng m^{-3}, with the highest value observed in the Atlantic (Table 1). Although East Asian aerosols showed the highest mean d-Fe concentrations, the contrast with marine aerosols was much smaller than that for T-Fe, suggesting that d-Fe concentrations in marine aerosols cannot be explained solely by the transport flux of Fe-bearing aerosols from continental source regions.

Fe_{sol}%, which strongly affects d-Fe concentrations, showed a wide range from 0.01% to 99.95% (mean: 9.76 ± 15.2%; median: 4.57%). Mean Fe_{sol}% was lowest in East Asia and higher in the North Pacific, reflecting the strong influence of East Asian outflow. By comparison, Fe_{sol}% in the South Pacific and Atlantic was lower than in the North Pacific, suggesting that these regions are less strongly affected by processes that enhance Fe_{sol}%. As in previous studies, Fe_{sol}% increased as T-Fe concentration decreased in all regions (Figure 2a; Sholkovitz et al., 2012; Mahowald et al., 2018). This inverse relationship was observed commonly over both land and ocean, indicating that it is a globally shared characteristic (Figure 2a). Previous studies suggest that this relationship mainly reflects (1) preferential removal of coarse mineral dust with low solubility relative to fine anthro-Fe with higher solubility, which increases the relative importance of anthro-Fe as aerosol concentrations decrease, and (2) increased Fe_{sol}% through chemical processing during atmospheric transport (Mahowald et al., 2018). The sources of d-Fe in aerosols from each region and basin were evaluated using the [d-Fe]/[d-Al]-$EF_{T\text{-}Fe}$ diagram. Many samples had $EF_{T\text{-}Fe}$ ratios less than 2.0 and [d-Fe]/[d-Al] ratios less than 1.0 (Figure 2b), suggesting that T-Fe was derived mainly from mineral

dust and that d-Fe was produced primarily through proton-promoted dissolution of those particles. Moreover, mean $F_{anthro\text{-}dFe}$ was less than 10% in all regions and basins, indicating that mineral dust-derived d-Fe is globally important for Fe supply to the ocean.

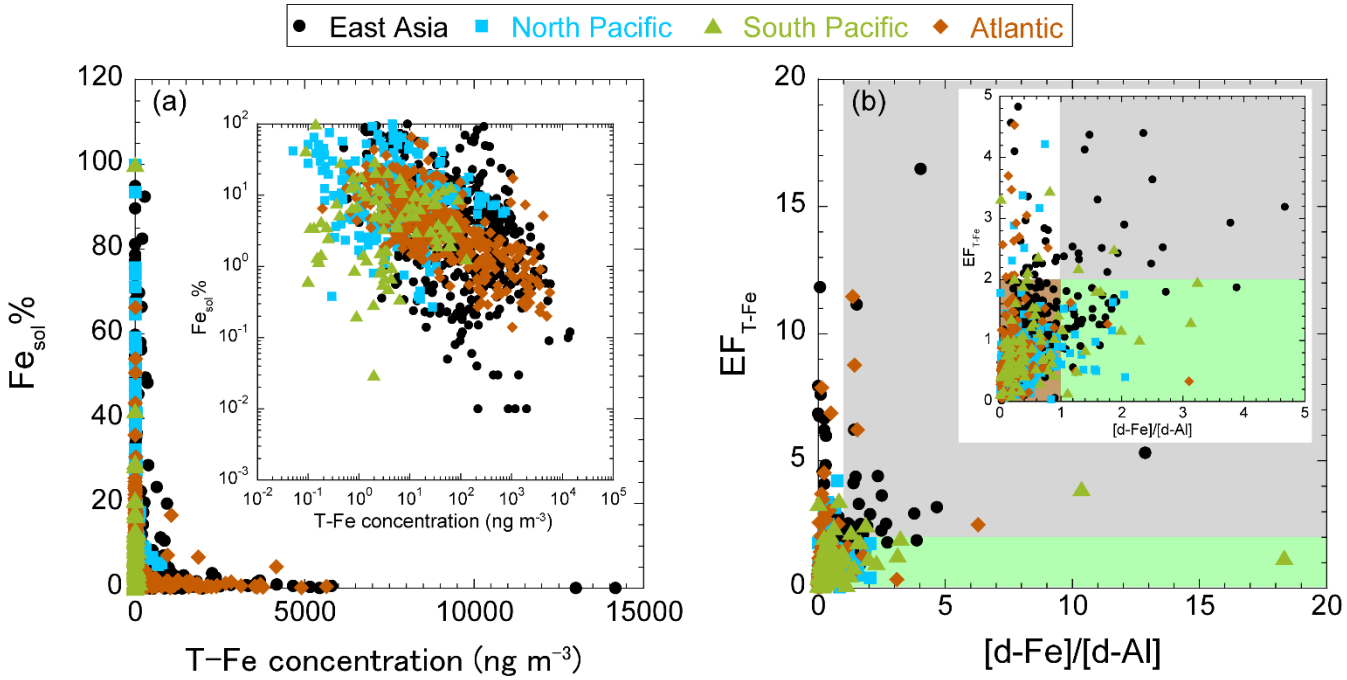

Figure 2. (a) Inverse plot of T-Fe concentration with Fe_{sol}% and (b) [d-Fe]/[d-Al]-$EF_{T\text{-}Fe}$ diagram in aerosol samples compiled by this study.

Table 1. Basin-scale summary of aerosol Fe sources, T-Fe and d-Fe concentrations, Fe solubility (Fe_{sol}%), and anthropogenic contribution to d-Fe ($f_{anthro\text{-}dFe}$) in TSPs. Values are presented as mean ± standard deviation, with ranges in parentheses. Figure numbers below each region refer to figures showing the spatial distributions of these values.

Area	T-Fe source(s)	d-Fe source(s)	Mean T-Fe conc. (ng m^{-3})	Mean d-Fe conc. (ng m^{-3})	Mean Fe_{sol}% (%)	Mean $f_{anthro\text{-}dFe}$ (%)
East Asia	**TSP and coarse aerosol**: Mineral dust **Fine aerosol**: Mineral dust + anthro-Fe	TSP and coarse: Fe dissolution from mineral dust Fine aerosols: Fe dissolution from mineral dust and anthro-Fe emitted as insoluble Fe	1101.3 ± 1861.7 (15.6–14166.7)	12.6 ± 27.0 (0.6–98.0)	3.5 ± 3.2 (0.1–17.5)	7.9 ± 10.3
N. Pacific (Figure 6)	Asian outflow of mineral dust	Fe dissolution from mineral dust: Fe_{sol}% in coarse aerosols were enhanced by chemical alteration in the marine atmosphere episodic anthro-Fe supply from shipping	50.0 ± 104.4 (0.2–764.5)	4.5 ± 7.3 (<0.1–45.9)	13.9 ± 14.4 (0.4–74.2)	6.1 ± 10.4
Atlantic (Figure 9)	Saharan dust	Fe dissolution from mineral dust: cloud processing in high altitude Anthro-Fe mostly insoluble	387.2 ± 922.9 (0.2–5650.0)	6.9 ± 23.4 (<0.1–212.7)	6.2 ± 6.8 (0.1–50.8)	5.1 ± 9.7
S. Pacific (Figure 12)	Mineral dust and volcanic influence near Heard Island	Coastal Australia aerosols affected by anthro emissions acidified aerosols. Volcanic influence near Heard Island	17.6 ± 25.3 (0.1–129.8)	1.0 ± 23.4 (<0.1–8.3)	7.3 ± 6.4 (<0.1–41.9)	Up to 20% near Australia. Apparent high values near Heard Island are driven by volcanic ash (not anthro-Fe).

References. East Asia: Duvall et al., 2008; Kurisu et al., 2019; Hsieh et al., 2023; Sakata et al., 2023, 2025; Seo and Kim, 2023. The North Pacific: Buck et al., 2006, 2013; Marsay et al., 2022; Sakata et al., 2022; Kurisu et al., 2024. The Atlantic Ocean: Baker et al., 2006a, 2006b, 2013, 2020; Buck et al., 2010a, 2010b; Chance et al., 2015. The South Pacific: Buck et al., 2013, 2019; Sakata et al., 2022; Perron et al., 2020a, 2021.

3.2 East Asian aerosols

3.2.1 Monthly trends of Fe and Al concentrations

Elevated T-Fe and T-Al concentrations were primarily observed from March to May (Figure 3a), consistent with the seasonal trend of Asian dust transport from the Gobi and Taklamakan Deserts, which peaks in March-May (Uematsu et al., 1983; Zhu et al., 2020; Kawai et al., 2021). T-Fe concentrations correlated strongly with T-Al concentrations in TSP samples (Figure S1a), and the mean $EF_{T\text{-}Fe}$ (1.6 ± 1.6; monthly mean: 1.2–1.9) was below 2.0, indicating that T-Fe in East Asian TSPs were mainly derived from mineral dust. Although the mean concentrations of T-Fe and T-Al were comparable in the coarse and fine fractions, their median concentrations tended to be higher in the coarse fraction (Figure S2a). Approximately 70% of aerosol Fe has previously been reported to reside in coarse aerosol particles (e.g., Kurisu et al., 2019; Sakata et al., 2023, 2025). However, these studies generally used a cutoff diameter of approximately 1.0 μm to separate coarse and fine particles. Under the size classification used in the present study, particles with diameters of 1.0–2.5 μm were included in the fine fraction. This difference in the cutoff diameter likely explains why the fine fraction accounted for a larger proportion of T-Fe in the present study than in previous studies.

The d-Fe and d-Al concentrations in TSP ranged from 0.6 to 98 ng m^{-3} and from 1 to 101 ng m^{-3}, respectively (Figure S1b). d-Fe concentrations were positively correlated with d-Al concentrations, suggesting that the two dissolved metals are influenced by similar processes (Figure S1b). Both d-Fe and d-Al concentrations tended to be higher in March-May, consistent with the seasonal patterns of T-Fe and T-Al (Figure 3b). This indicated that the atmospheric loading of mineral dust and anthropogenic aerosols was an important factor influencing d-Fe variability. However, no significant correlations were found between T-Fe and d-Fe, or between T-Al and d-Al (Figures S1c and S1d), indicating that total elemental loading alone cannot explain the variability in dissolved metal concentrations. In contrast to T-Fe and T-Al, fine aerosol particles exhibited higher mean concentrations of d-Fe and d-Al than coarse aerosol particles (Figure S2a). These findings highlighted the important role of fine aerosol particles in supplying Fe to surface seawater via atmospheric deposition.

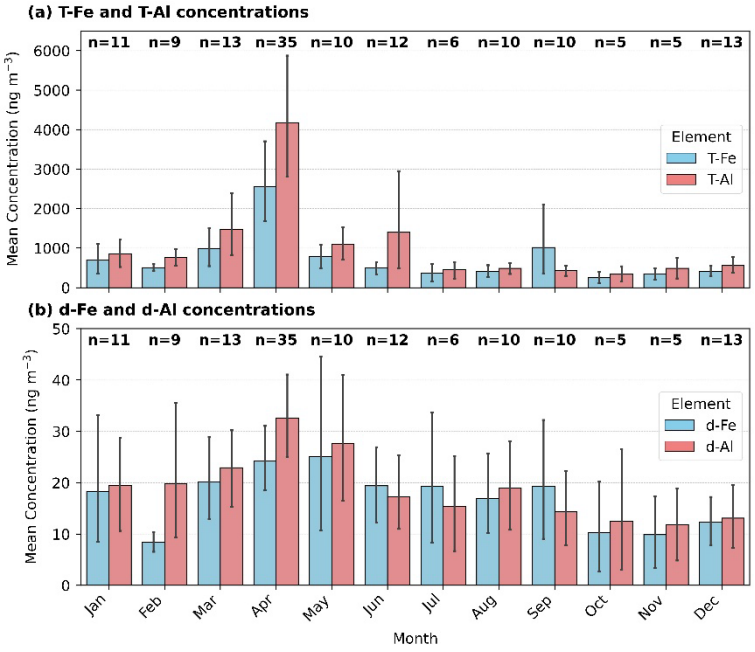

Figure 3. Monthly mean concentrations of (a) T-Fe and T-Al, and (b) d-Fe and d-Al in East Asian TSP.

3.2.2 Factors controlling Fe_{sol}% of East Asian TSP

The annual mean Fe_{sol}% in East Asian TSP was 3.5 ± 3.2%, ranging from 0.1% to 17.5%, and tended to be higher during June–August (Figure 4a). Both mineral-Fe_{sol}% and anthro-Fe_{sol}% showed similar seasonal patterns of Fe_{sol}%, although the solubility of anthro-Fe was lower than that of mineral-Fe (Figure 4a). Despite lower anthro-Fe_{sol}% than mineral-Fe_{sol}%, anthro-dFe also increased during June–August, indicating that anthro-Fe may have partly contributed to the seasonal variation in bulk Fe_{sol}%. Nevertheless, the annual mean $f_{anthro\text{-}dFe}$ in TSP was only 7.9 ± 10.3% (Figure 5a). Accordingly, most East Asian TSP samples plotted within areas (i) and (iii) of the [d-Fe]/[d-Al]–$EF_{T\text{-}Fe}$ diagram (Figure 5b). This distribution indicates that T-Fe originated primarily from mineral dust and poorly soluble anthro-Fe, whereas d-Fe was derived mainly from proton-promoted dissolution of mineral dust, with only a limited contribution from anthro-Fe.

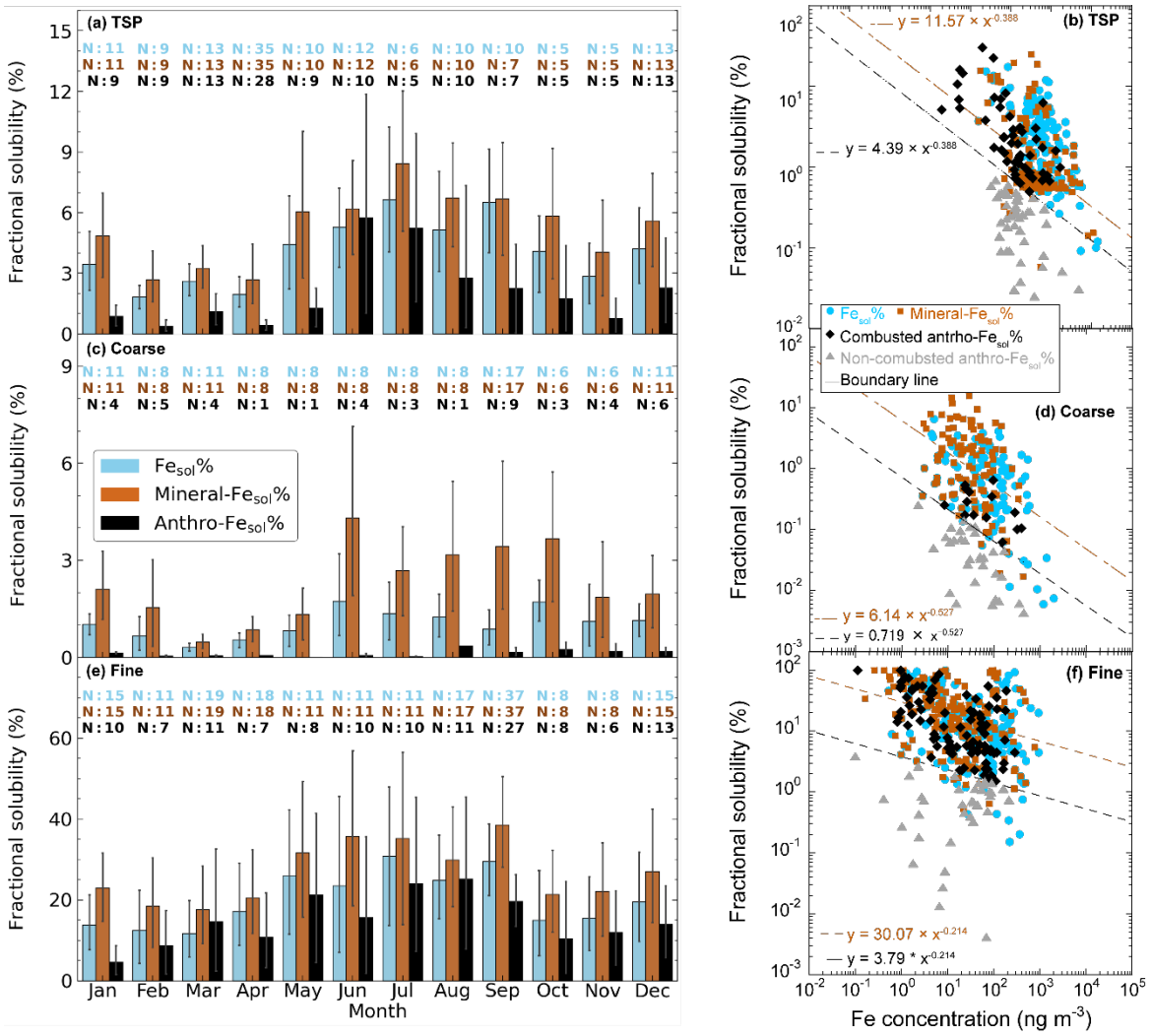

Figure 4. (a) Monthly variations in Fe_{sol}%, mineral-Fe_{sol}%, and anthro-Fe_{sol}% for TSP, and (b) their relationships with Fe concentration. (c, d) Same as (a, b), but for coarse aerosol particles. (e, f) Same as (a, b), but for fine aerosol particles. Cyan circles, orange squares, black diamonds, and gray triangles represent Fe_{sol}%, mineral-Fe_{sol}%, combusted anthro-Fe_{sol}%, and non-combusted anthro-Fe_{sol}%, respectively. Brown dashed lines indicate the power-law fits for mineral-Fe_{sol}%, whereas black dashed lines denote the boundaries separating combusted and non-combusted anthro-Fe.

To investigate the mechanism underlying the inverse relationship between Fe_{sol}% and T-Fe concentration, the variations in mineral-Fe_{sol}% and anthro-Fe_{sol}% with their respective Fe concentrations were examined. If this inverse relationship were governed solely by mixing between mineral dust with low Fe_{sol}% and highly soluble anthro-Fe, neither mineral-Fe_{sol}% nor anthro-Fe_{sol}% would be expected to depend on concentration. However, both mineral-Fe_{sol}% and anthro-Fe_{sol}% increased as

Fe concentration decreased (Figure 4b). These results indicate that the inverse relationship between Fe_{sol}% and T-Fe in East Asian TSP cannot be explained by simple source mixing alone, but instead reflects enhanced Fe dissolution of both mineral dust and anthro-Fe during chemical processing during the atmospheric transport. To evaluate regional differences, two-sided Mann–Whitney U tests with Holm correction were applied because the data were not normally distributed. The analysis showed that TSP collected in Japan during the Asian outflow season exhibited significantly higher Fe solubility than those collected in China and Korea: bulk Fe_{sol}% for the TSP samples collected in Japan (mean ± SD = 4.9 ± 3.6%) was higher than those in China and Korea (= 2.5 ± 2.5%; Holm-adjusted p = 0.0017). Significant differences were also observed for mineral-Fe_{sol}% (Japan: 6.2 ± 3.5%, China and Korea: 3.2 ± 4.1%; Holm-adjusted p = 0.0012) and anthro-Fe_{sol}% (Japan: 2.5 ± 4.2%, China and Korea: 0.9 ± 1.2%; Holm-adjusted p = 0.0057). Together, these results support the progressive solubilization of both mineral-Fe and anthro-Fe during transport from the East Asian continent.

Anthro-Fe_{sol}% in East Asian TSP exhibited a wider variation than mineral-Fe_{sol}% (Figure 4b). Although combustion-derived anthro-Fe is generally considered to be more soluble than mineral-Fe, some samples showed anthro-Fesol% lower than mineral-Fe_{sol}% and below 0.1%, the approximate lower limit reported for combustion-derived Fe. Such low-solubility anthro-Fe was likely derived from sources other than high-temperature combustion. To account for changes in the solubility of mineral-Fe and anthro-Fe during atmospheric transport, the use of a fixed threshold such as 0.1% was avoided. Instead, a boundary line parallel to and below the log–log regression line between mineral-Fe concentration and mineral-Fesol% was defined so that 5% of the mineral-Fe samples fell below it. For each mineral-Fe sample, the relative deviation from the regression relationship was quantified as the logarithm of the observed-to-predicted mineral-Fe_{sol}% ratio [log(observed mineral-Fe_{sol}%/predicted mineral-Fe_{sol}%)]. The 5th percentile of these relative deviations was then added to the intercept of the regression equation to define the boundary line. Based on this boundary, anthro-Fe samples below the boundary line were operationally classified as non-combusted anthro-Fe, whereas those above the line were classified as high-temperature combustion-derived anthro-Fe, with solubility comparable to or higher than that of mineral-Fe (Figure 4b).

In the non-combusted anthro-Fe group below the boundary, all anthro-Fe_{sol}% values were below 1.0%, with an average of 0.3 ± 0.2%. Several samples with high anthro-Fe concentrations showed particularly low values of less than 0.1%. Such low solubility is consistent with non-combusted anthro-Fe, including Fe associated with brake-pad debris and tire-wear particles (Halle et al., 2013; Shupert et al., 2021; Cui et al., 2025). By contrast, the high-temperature combustion-derived anthro-Fe group above the boundary had an average anthro-Fe_{sol}% of 4.0 ± 5.7%, higher than the average mineral-Fe_{sol}% of 2.4 ± 4.1% in East Asian TSP. This characteristic is consistent with the generally higher solubility of anthro-Fe derived from high-temperature combustion. However, anthro-Fe_{sol}% was generally only approximately 1% even in high-concentration samples dominated by relatively fresh aerosol particles. This observation implies that these particles were emitted with relatively low initial solubility rather than in a highly soluble form and that they subsequently underwent solubilization through chemical processing during atmospheric transport (Sholkovitz et al., 2009; Ito et al., 2021).

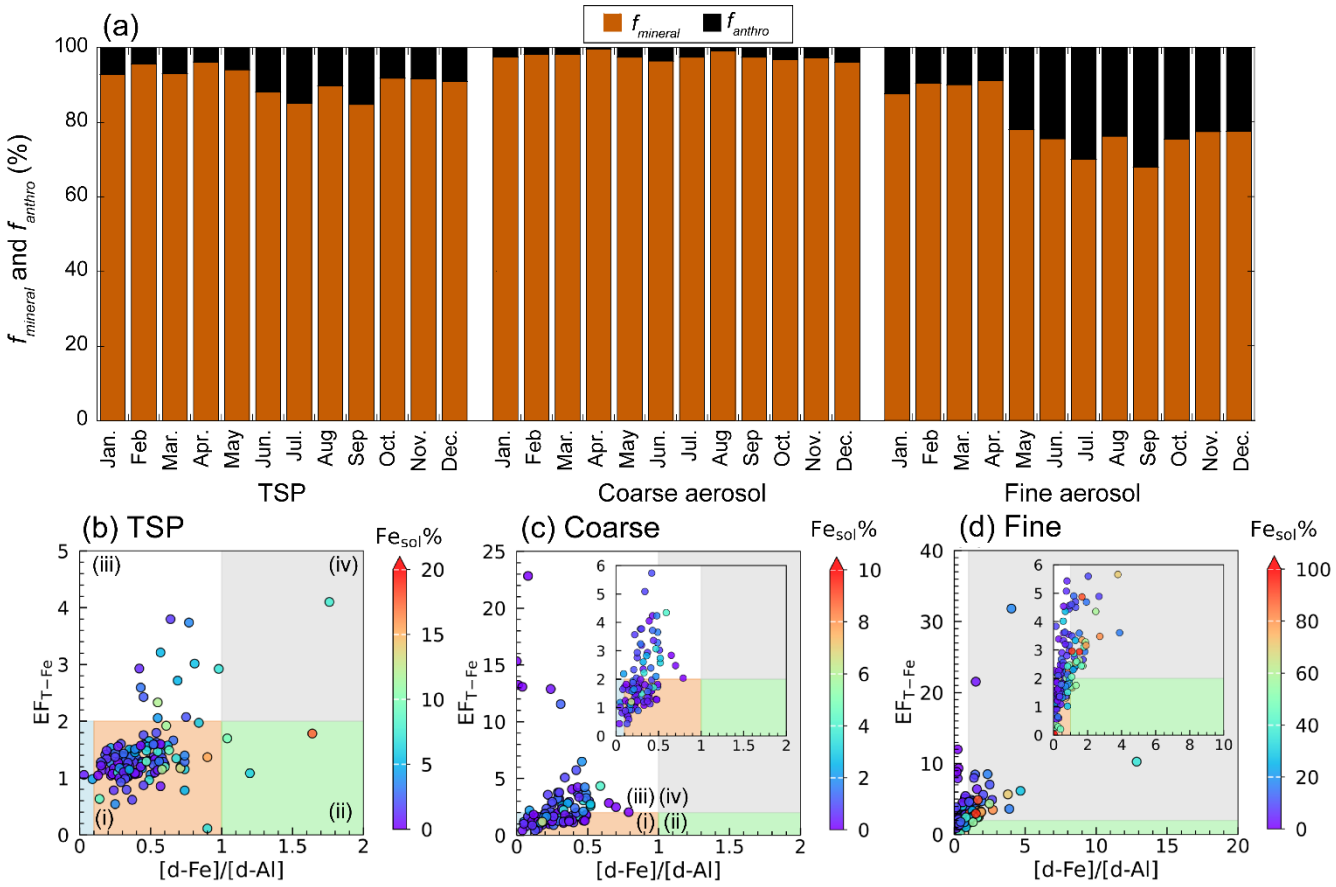

Figure 5. Diagrams between [d-Fe]/[d-Al] and $EF_{T\text{-}Fe}$ in (a) TSPs, (b) coarse aerosol particles and (c) fine aerosol particles and their magnified figures. (d) Monthly trends of $f_{mineral\text{-}dFe}$ and $f_{anthro\text{-}dFe}$ in TSP, coarse and fine aerosol particles.

3.2.3 Factors controlling Fe_{sol}% of East Asian coarse aerosol particles

The mean Fe_{sol}% in coarse aerosol particles was 1.0 ± 1.1%, with higher values observed from June to August (Figure 4c). This value was lower than the mean mineral-Fe_{sol}% of 2.3 ± 2.9% but higher than the mean anthro-Fe_{sol}% of 0.1 ± 0.2% (Figure 4c). As observed for TSP, most coarse aerosol samples were distributed within regions (i) and (iii) of the [d-Fe]/[d-Al]–$EF_{T\text{-}Fe}$ diagram (Figure 5c). These results indicate that T-Fe in East Asian coarse aerosol particles was derived primarily from mineral dust and poorly soluble anthro-Fe, whereas d-Fe was supplied mainly through proton-promoted dissolution of mineral dust. Indeed, the contribution of anthro-Fe to d-Fe in coarse aerosol particles remained low throughout the year, with an annual mean of only 2.4 ± 3.9% (Figure 5a).

Even in coarse aerosol particles, mineral-Fe_{sol}% increased with decreasing mineral-Fe concentration (Figure 4d). Because there is little reason to assume multiple mineral-dust endmembers with different initial Fe_{sol}% values, this inverse

relationship is interpreted as resulting not from simple mixing but from the combined effects of chemical processing during atmospheric transport and depositional removal. The mean mineral-Fe_{sol}% in coarse aerosol particles was 2.3 ± 2.9%, slightly exceeding the range reported for fresh mineral dust (Duvall et al., 2008; Shi et al., 2011a; Desboeufs et al., 2001). However, mineral dust in coarse aerosol particles occurs predominantly as crystalline aluminosilicates and contains relatively high proportions of alkaline minerals such as calcite ($CaCO_3$), making coarse particles less susceptible to strong acidification than fine aerosol particles. Proton-promoted Fe dissolution from Fe-bearing aluminosilicates is generally considered to proceed only after the buffering capacity of $CaCO_3$ has been depleted. Nevertheless, $CaCO_3$ is known to remain in coarse particles even after transport from the Gobi and Taklamakan deserts to Japan (Meskhidze et al., 2005; Fairlie et al., 2010; Takahashi et al., 2009; Miyamoto et al., 2020). Substantial Fe solubilization through aerosol acidification is therefore unlikely in coarse aerosol particles. Instead, the modest increase in the observed mineral-Fe_{sol}% was likely attributable to the partial transformation of Fe in chlorite and biotite into ferrihydrite and Fe(II, III) sulfates (Takahashi et al., 2011; Sakata et al., 2025).

Most anthro-Fe in coarse aerosol particles was distributed below the boundary line separating combusted from non-combusted anthro-Fe, and the low-solubility group exhibited an extremely low mean anthro-Fe_{sol}% of 0.05 ± 0.05% (Figure 4). These particles likely corresponded primarily to non-combustion anthro-Fe, including resuspended non-exhaust vehicle particles and slag originating from raw-material and by-product storage areas at steel-production facilities (Harrison et al., 2012; Kajino et al., 2020; Kurisu et al., 2019, 2026). Because Fe in these particles occurs mainly as Fe oxides, which are less soluble than Fe in aluminosilicates under weakly acidic to neutral conditions, its contribution to d-Fe in coarse aerosol particles was likely limited (Journet et al., 2008; Shupert et al., 2013; Halle et al., 2021; Cui et al., 2025).

3.2.4 Factors controlling Fe_{sol}% of East Asian fine aerosol particles

The annual mean bulk Fe_{sol}% in fine aerosol particles was 21.1 ± 23.6%, approximately one order of magnitude higher than that in coarse aerosol particles (1.0 ± 1.1%) (Figure 4c, e). In fine aerosol particles, both mineral-Fe_{sol}% (mean: 27.9 ± 28.0%) and anthro-Fe_{sol}% (mean: 16.0 ± 22.3%) exceeded 10% (Figure 4e), corresponding to higher d-Fe concentrations than those in coarse aerosol particles (Figure S2a). Unlike TSP and coarse aerosol particles, fine aerosol particles were plotted in area (iv), indicating that anthro-Fe with high Fesol% contributed to d-Fe sources (Figure5d). Indeed, the fraction of d-Fe derived from anthro-Fe averaged 21.0 ± 26.3% and was therefore not negligible (Figure 5a). Nevertheless, anthro-Fe_{sol}% was lower than mineral-Fe_{sol}% (Figure 4e) due to the presence of insoluble anthro-Fe plotted in area (iii) (Figure 5d). Most anthro-Fe in fine aerosol particles was distributed above the boundary separating combusted from non-combusted anthro-Fe, although the contribution of anthro-Fe below the boundary was also non-negligible (Figure 4f). This distribution indicates that fine aerosol particles contained not only highly soluble combusted anthro-Fe but also poorly soluble non-combusted anthro-Fe. The contribution of the latter likely partly explains why anthro-Fe_{sol}% was lower than mineral-Fe_{sol}% in fine aerosol particles.

In fine aerosol particles, both mineral-Fe_{sol}% and combusted anthro-Fe_{sol}% increased with decreasing concentrations of their respective Fe components, providing clear evidence that both components underwent solubilization during atmospheric

transport (Figure 4f). This likely reflects the large specific surface area of fine aerosol particles and their greater susceptibility to reactions with acidic species and organic ligands. Fine aerosol particles are particularly susceptible to acidification because their pH is generally more than one unit lower than that of coarse aerosol particles, which retain $CaCO_3$ (Guo et al., 2018; Pye et al., 2020). Consistent with this interpretation, single-particle analyses have identified sulfate coatings on both mineral dust and anthro-Fe in fine aerosol particles, and Fe(III)-sulfates have been detected in TSP and fine aerosol particles collected in Japan (Sullivan et al., 2007; Li et al., 2017; Zhu et al., 2022; Takahashi et al., 2013; Sakata et al., 2025). Furthermore, Fe(III)-sulfates form under highly acidic conditions (pH < 3.0), and $CaCO_3$ has not been detected in fine aerosol particles in Japan, suggesting that acidification of poorly buffered fine particles strongly promoted Fe dissolution (Meskhidze et al., 2005; Fairlie et al., 2010; Miyamoto et al., 2020; Sakata et al., 2022). In both coarse and fine aerosol particles, mineral-Fe_{sol}% and anthro-Fe_{sol}% were elevated from June to August, consistent with the lower aerosol pH and higher [nss-SO_4^{2-}]/[T-Fe] ratios observed during this season (Tao and Murphy, 2019b; Pye et al., 2020; Song and Osada, 2020; Sakata et al., 2025). These results indicate that acidification was the dominant factor controlling the solubilization of both mineral dust and anthro-Fe in fine aerosol particles. Although anthro-Fe emitted from heavy-oil combustion is known to exhibit Fe_{sol}% values exceeding 30% at the time of emission, samples with anthro-Fe_{sol}% above 30% were uncommon in this study (Sedwick et al., 2007; Schroth et al., 2009; Oakes et al., 2012; Ito et al., 2021). This suggests that anthro-Fe derived from solid-fuel combustion and high-temperature industrial processes, such as coal combustion and steel production, contributed more strongly than highly soluble anthro-Fe from liquid-fuel combustion, such as heavy-oil and gasoline combustion.

In the group below the boundary, anthro-Fe_{sol}% was frequently below 0.1%, with a mean value of 0.9 ± 0.8%. As inferred for coarse aerosol particles, this group likely reflected the influence of non-combustion anthro-Fe, including brake-pad and tire-wear debris in non-exhaust vehicle particles (Kajino et al., 2020; Sakata et al., 2025). Because the maximum anthro-Fesol% in this group was only 3.7%, it was likely composed of Fe species that are intrinsically resistant to atmospheric solubilization. These results suggest that combusted and non-combusted anthro-Fe differ markedly not only in their initial solubility but also in their reactivity toward solubilization during atmospheric transport.

3.3 The North Pacific Ocean

3.3.1 Monthly and spatial trend of T-Fe and d-Fe concentration

The North Pacific is strongly influenced by aerosol outflow from East Asia, particularly mineral dust transported from the Asian continent. T-Fe and T-Al concentrations in North Pacific TSPs ranged from 0.2 to 764.5 ng m^{-3} and 0.4 to 1320.7 ng m^{-3}, respectively. T-Fe was strongly correlated with T-Al, and the slope of the regression line was comparable to the T-Fe/T-Al ratio characteristic of mineral dust (Figure S3a). This suggests that T-Fe in North Pacific TSPs was primarily derived from mineral dust, consistent with the near-unity mean $EF_{T\text{-}Fe}$ value (1.3 ± 1.2). Concentrations of d-Fe and d-Al ranged from <0.1 to 45.9 ng m^{-3} and 0.1 to 70.8 ng m^{-3}, respectively, with d-Fe showing a strong correlation with d-Al (Figure S3b). The

mean [d-Fe]/[d-Al] ratio of 0.39 ± 0.29 aligns with values for mineral dust subjected to proton-promoted dissolution (Figure S4a). These results indicate that both T-Fe and d-Fe in North Pacific TSPs largely originated from mineral dust.

Distinct from East Asian aerosols, North Pacific aerosols exhibited strong correlations between d-Fe and T-Fe concentrations, as well as between d-Al and T-Al concentrations (Figure S3c and S3d). This suggests that the amount of d-Fe supplied to the North Pacific is primarily controlled by the total transport flux of T-Fe-containing aerosols. Shipboard observations revealed that T-Fe and d-Fe concentrations in the marine boundary layer decreased with increasing distance from East Asia (Figures 6a and 6b), indicating the deposition of T-Fe and d-Fe-containing particles from the atmosphere to the ocean during transport. Furthermore, the highest T-Fe and d-Fe concentrations were observed in March–May, coinciding with the period of mineral dust transport from the Gobi and Taklamakan deserts (Figures 7a and 7b).

This spatial and seasonal pattern is broadly consistent with satellite-derived dust aerosol optical depth (DAOD), a proxy for the atmospheric column abundance of mineral dust (Song et al., 2021). Satellite observations also show enhanced surface seawater chlorophyll a following dust events over the North Pacific (Luo et al., 2020; Yoon et al., 2022), suggesting that continental mineral dust is an important source of d-Fe supporting biological primary production in this region. These results highlight the importance of understanding both the seasonality of Fe emission sources and the processes controlling Fe_{sol}% in North Pacific aerosols.

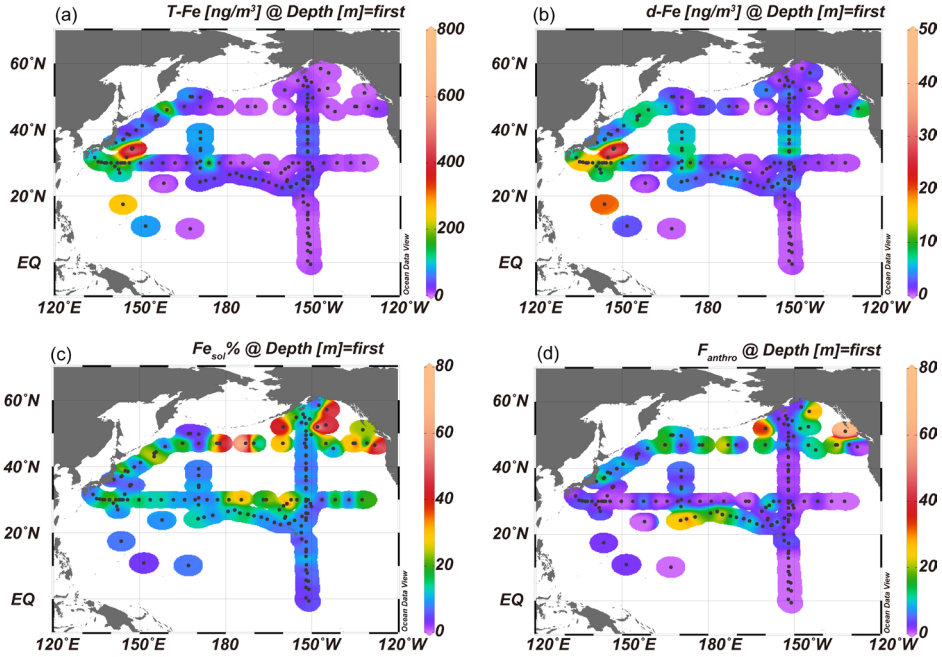

Figure 6. Spatial distributions of (a) T-Fe concentration, (b) d-Fe concentration, (c) Fe_{sol}%, and (d) $f_{anthro\text{-}dFe}$ in the North Pacific TSP samples.

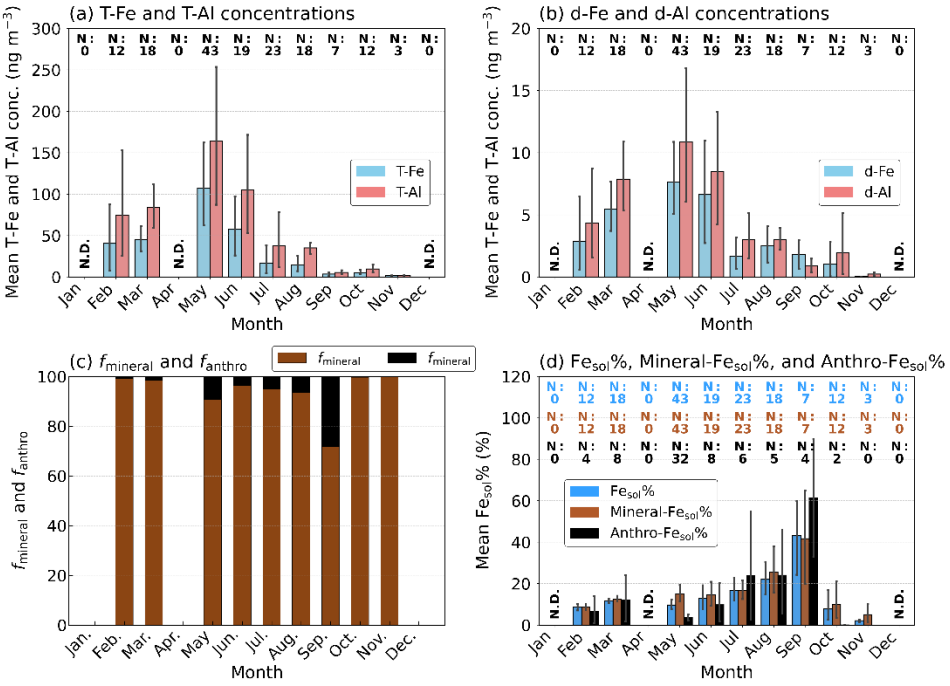

Figure 7. Monthly trends of (a) T-Fe concentration, (b) d-Fe concentration, (c) Fe_{sol}%, and (d) $f_{anthro\text{-}dFe}$ in the North Pacific TSP samples.

3.3.2 The impact of anthro-Fe on Fe_{sol}% in the North Pacific aerosols

Figure S4a shows the relationship between [d-Fe]/[d-Al] and $EF_{T\text{-}Fe}$ in North Pacific TSP samples. Consistent with the mineral dust dominance described above, most samples were distributed within the proton-promoted dissolution regime for mineral dust (area (i) in Figure S4a). Nevertheless, several samples exhibited $EF_{T\text{-}Fe}$ values greater than 2.0, indicating that anthro-Fe contributed to T-Fe in North Pacific aerosols. Moreover, 67 of the 155 samples had a detectable anthro-Fe contribution to d-Fe ($f_{anthro\text{-}dFe} > 0$). Among these, 37 samples had $f_{anthro\text{-}dFe}$ values above 10% (maximum: 73.7%), indicating that anthro-Fe contribution to d-Fe cannot be negligible in at least some North Pacific aerosols.

Following the same approach used for East Asia, anthro-Fe was further classified into combusted anthro-Fe (33 samples) and non-combusted anthro-Fe (34 samples) according to whether anthro-Fe_{sol}% overlapped with mineral-Fe_{sol}% at similar Fe concentrations (Figure 8a). Most samples below the boundary were collected from February to May, when East Asian outflow is strong, suggesting a substantial influence of continental anthropogenic emissions. Their mean anthro-Fe_{sol}% was 1.0 ± 0.8%, and although anthro-Fe_{sol}% increased slightly with decreasing concentration, the maximum value was only 2.7%. These particles occurred in both coarse and fine aerosol particles, and their persistently low solubility resembled that of non-exhaust vehicle particles such as brake-pad debris (Figures 8b and 8c). Accordingly, non-combusted anthro-Fe, including non-exhaust

vehicle particles, likely remains largely insoluble even after long-range transport over the marine atmosphere and probably contributes little to d-Fe supply in the North Pacific.

By contrast, anthro-Fe in TSP plotted above the boundary showed a high mean anthro-Fe_{sol}% of 23.2 ± 26.5% (Figure 8a). These particles occurred predominantly in fine aerosol particles, with only minor contributions in the coarse fraction (Figures 8b and 8c), suggesting a primary association with high-temperature combustion sources. During February to May, when East Asian outflow is strongest, anthro-Fe_{sol}% in this group tended to be lower than the overall mean, consistent with a substantial contribution from East Asia-derived solid-fuel combustion, for which anthro-Fe_{sol}% at emission is not necessarily high. In contrast, during June-August, particularly in September when the influence of Asian outflow weakened, combusted anthro-Fe often showed anthro-Fe_{sol}% values higher than the mean for samples above the boundary separating non-combusted and combusted anthro-Fe. This pattern likely contributed to the enhanced influence of anthro-Fe in TSP during this period (Figure 7c). One plausible seasonal source is heavy-oil combustion from ship traffic along the major shipping route linking East Asia and North America. A previous modeling study estimated that approximately 40% of d-Fe in North Pacific aerosols was derived from ship emissions (Ito, 2013), and ship emissions are known to contain highly soluble Fe at emission (Fe_{sol}% > 30%; Schroth et al., 2009; Oakes et al., 2012). Thus, ship-related anthro-Fe may efficiently enhance Fe_{sol}% in June-August. However, because d-Fe concentrations in North Pacific aerosols were lower in June-August than in other seasons (Figures 7b and 7d), the annual contribution of ship-related anthro-Fe to total d-Fe deposition is likely limited.

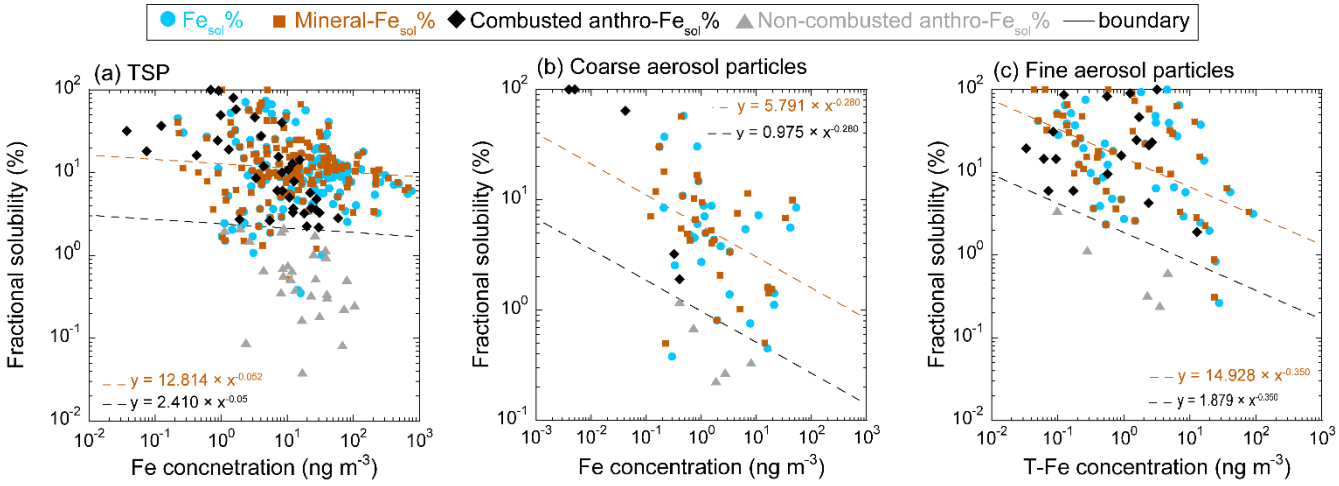

Figure 8. Inverse relationships between T-Fe, mineral-Fe, and anthro-Fe and their respective Fe solubilities in (a) TSP, (b) coarse aerosol particles, and (c) fine aerosol particles collected in the North Pacific. Brown dashed lines indicate the power-law fits for mineral-Fe_{sol}%, whereas black dashed lines denote the boundaries separating combusted and non-combusted anthro-Fe.

3.3.3 The impact of chemical alterations on Fe_{sol}% in the North Pacific aerosols

The mean Fe_{sol}%, mineral-Fe_{sol}%, and anthro-Fe_{sol}% in North Pacific TSP were higher than those in East Asian aerosols collected during winter and spring, when Asian outflow is strongest (Table 2). This suggests that aerosols transported from East Asia undergo further chemical alteration during transport over the North Pacific. Size-resolved comparisons showed that both mineral-Fe_{sol}% and anthro-Fe_{sol}% increase in coarse aerosol particles during transport from Japan to the North Pacific, whereas no pronounced changes were observed in fine aerosol particles. A similar pattern was observed for Al_{sol}%, an indicator of mineral-dust alteration. Al_{sol}% in TSP and coarse aerosol particles was higher over the North Pacific than in Japan, whereas no pronounced difference was observed for fine aerosol particles between Japan and the North Pacific (Table 2). Although size-dependent differences in the mineralogical composition of source dust may potentially affect Fe solubility, differences in Fe_{sol}% appear to be minimal for freshly emitted mineral dust (Shi et al., 2011a). Additional input of anthro-Fe from ship-derived heavy-oil combustion may provide highly soluble Fe to the marine atmosphere (Sedwick et al., 2007). However, such emissions are expected to affect mainly fine aerosol particles and therefore cannot fully explain the preferential increase in solubility observed in coarse aerosol particles. Thus, the concurrent increases in mineral-Fe_{sol}% and Al_{sol}% in coarse aerosol particles suggest that mineral dust undergoes further chemical alteration during transport through the marine atmosphere. In contrast, the absence of substantial changes in solubility in fine aerosol particles between East Asia and the North Pacific suggests that their alteration pathway differs from that of coarse aerosol particles. Given that fine aerosol particles generally have larger specific surface areas and are therefore expected to be more reactive than coarse aerosol particles, the pronounced increases in Fe_{sol}% and Al_{sol}% specifically in coarse aerosol particles are particularly notable and require further explanation.

Focusing first on fine aerosol particles, the similarity in Fe_{sol}% between East Asia and the North Pacific suggests that substantial Fe solubilization in this size fraction had already occurred during the early stages of transport within East Asia, rather than during subsequent long-range transport over the North Pacific (Table 2). Such rapid Fe dissolution was likely promoted by strongly acidic conditions during transport from China to Japan. This interpretation is consistent with kinetic models showing rapid initial Fe dissolution followed by an approach to a plateau (Shi et al., 2011b). It is also consistent with previous applications of such models, which indicate that Fe dissolution in fine aerosol particles over the Sea of Japan and the North Pacific is already close to this plateau stage (Shi et al., 2011b, 2015; Maters et al., 2016; Sakata et al., 2022, 2025). Thus, additional acidification during subsequent marine transport would not be expected to produce a large further increase in Fe_{sol}%. However, aerosol particles likely underwent cloud processing during marine transport. In the absence of organic complexation, such processing would favor ferrihydrite precipitation under moderately acidic conditions, where inorganic Fe solubility is low, approximately pH > 4.0–6.0 (Pye et al., 2020). The persistence of high Fe_{sol}% during marine transport therefore implies that dissolved Fe is stabilized against removal. Complexation with organic ligands is a plausible mechanism, as strong Fe-binding ligands can keep Fe soluble after dissolution. Supporting this idea, Wu et al. (2023) showed that the Fe_{sol}% of fine aerosol particles collected on Matsu Island remained high for 10 days in seawater amended with deferoxamine, whereas it decreased to below 1% without deferoxamine. This finding suggests that strong organic ligands can prevent the decrease in Fe

solubility and maintain dissolved Fe over extended periods. Consistent with this interpretation, previous studies have reported or suggested organic ligands capable of stabilizing Fe(II) and/or Fe(III) in marine and coastal rainwater. Microorganisms in cloud water have also been suggested to produce siderophores, a class of strong Fe-binding ligands (Kieber et al., 2003; Willey et al., 2008; Cheize et al., 2012; Vinatier et al., 2016). Fe(III)-HULIS complexes have also been detected in fine aerosol particles over the North Pacific (Sakata et al., 2022; Kurisu et al., 2024). Because these Fe-organic complexes can remain soluble over a wide pH range, organic ligands present in cloud water may help preserve d-Fe during cloud processing and suppress the decrease in Fe solubility that would otherwise occur in the absence of strong organic ligands.

By contrast, aerosol acidification is unlikely to be the main reason for elevated Fe_{sol}% in coarse aerosol particles over the North Pacific, because previous modeling studies have suggested that calcite buffering remains effective during transport, and charge-balance calculations likewise indicate that coarse aerosol particles over the North Pacific do not contain sufficient acidity to exhaust the buffering capacity of calcite (Meskhidze et al., 2005; Ito and Feng, 2010; Fairlie et al., 2010; Sakata et al., 2022). In the case of coarse aerosol particles, organic ligands may have contributed not only to the stabilization of Fe that had already been released into the dissolved fraction but also to further Fe dissolution from aerosol particles, because a larger fraction of low-solubility mineral Fe likely remained. Indeed, several coarse aerosol samples in this study were plotted in area (ii) of the [d-Fe]/[d-Al]–$EF_{T\text{-}Fe}$ diagram, where d-Fe is interpreted to be supplied mainly by ligand-promoted dissolution of mineral dust, and these samples showed a high mean Fe_{sol}% of 39.9 ± 22.4%. Experimental results from Wu et al. (2023) support this interpretation, showing that the Fe_{sol}% of coarse aerosol particles from Matsu Island increased from a few percent to about 10% in the presence of a strong Fe-binding ligand under seawater pH conditions. These results indicate that coarse aerosol particles retain a pool of Fe that can undergo further ligand-promoted dissolution. This interpretation is also consistent with the inter-laboratory comparison of Tang et al. (2025), which showed that, under the stronger leaching conditions of the Berger method, the increase in Fe_{sol}% relative to ultrapure water extraction was larger than that in Al_{sol}%. Such preferential enhancement of Fe relative to Al dissolution can increase [d-Fe]/[d-Al] ratios. Although the number of such samples was limited, the coexistence of high Fe_{sol}% and high [d-Fe]/[d-Al] ratios suggest that organic ligands in the marine atmosphere can enhance Fe dissolution from coarse aerosol particles during transport. Nevertheless, more direct observational evidence is needed to constrain the importance of this process over the North Pacific.

Table 2. Annual and December–May means of Fe_{sol}, mineral-Fe_{sol}, anthro-Fe_{sol}, and $f_{anthro\text{-}dFe}$ in total suspended particles (TSP), coarse aerosol particles, and fine aerosol particles collected in East Asia and the North Pacific. Values are given as mean ± standard deviation, with the number of samples (N) shown in parentheses. Italicized values denote means calculated from 10 or fewer samples (N ≤ 10) and should be interpreted with caution because of their greater uncertainty.

Variable	Period	TSP		Coarse aerosol particles		Fine aerosol particles	
		East Asia	North Pacific	East Asia	North Pacific	East Asia	North Pacific
Fe_{sol}%	Annual	3.5 ± 3.2 (N = 139)	13.9 ± 14.4 (N = 155)	1.0 ± 1.0 (N = 110)	9.2 ± 12.8 (N = 31)	21.0 ± 23.6 (N = 181)	24.3 ± 24.9 (N = 47)
	Dec.–May	2.8 ± 2.7 (N = 91)	10.5 ± 6.5 (N = 73)	0.8 ± 0.7 (N = 57)	*6.0 ± 4.6 (N = 10)*	16.3 ± 19.3 (N = 86)	13.1 ± 16.4 (N = 20)
Mineral-Fe_{sol}%	Annual	4.7 ± 4.5 (N = 137)	16.3 ± 16.6 (N = 155)	2.3 ± 2.9 (N = 110)	8.9 ± 11.0 (N = 31)	27.9 ± 28.0 (N = 181)	28.5 ± 28.7 (N = 47)
	Dec.–May	3.8 ± 4.2 (N = 91)	13.4 ± 10.7 (N = 73)	2.8 ± 2.7 (N = 57)	*4.8 ± 10.0 (N = 10)*	22.5 ± 23.4 (N = 86)	15.2 ± 18.1 (N = 20)
Anthro-Fe_{sol}%	Annual	1.7 ± 4.1 (N = 91)	12.1 ± 21.8 (N = 69)	0.1 ± 0.2 (N = 45)	*11.3 ± 30.2 (N = 10)*	16.0 ± 22.4 (N = 56)	26.2 ± 32.0 (N = 23)
	Dec.–May	1.0 ± 2.0 (N = 81)	5.4 ± 8.9 (N = 44)	0.1 ± 0.1 (N = 21)	*0.9 ± 3.0 (N = 3)*	12.3 ± 20.1 (N = 181)	*17.4 ± 27.5 (N = 8)*
Al_{sol}%	Annual	2.9 ± 2.4 (N = 139)	10.5 ± 9.3 (N = 155)	2.2 ± 2.5 (N = 110)	11.8 ± 16.2 (N = 31)	16.3 ± 15.0 (N = 181)	20.2 ± 17.0 (N = 47)
	Dec.–May	2.5 ± 2.6 (N = 91)	8.5 ± 5.1 (N = 73)	1.5 ± 1.8 (N = 57)	*11.4 ± 15.3 (N = 10)*	13.2 ± 11.7 (N = 86)	13.5 ± 13.1 (N = 20)

3.4 The Atlantic aerosols

3.4.1 Spatial and monthly trend of T-Fe and d-Fe concentrations

The T-Fe and T-Al concentrations in the Atlantic TSPs ranged from 0.2 to 5650.0 ng m^{-3} and from 0.8 to 7485.0 ng m^{-3}, respectively. The high concentration of T-Fe was mainly found in the coastal region of the Saharan Desert extending to 20–30°W between 10–20°N (Figure 9a). T-Fe concentration in the Atlantic TSPs was correlated with T-Al concentration and the slope of its regression line closely matched T-Fe/T-Al ratio of mineral dust (r: 0.60, Figure S5a). Indeed, the mean value of $EF_{T\text{-}Fe}$ was 1.5 ± 1.7, indicating that mineral dust is the most dominant source of T-Fe in the Atlantic TSPs.

Concentrations of d-Fe and d-Al ranged from <0.1 to 212.7 ng m^{-3} and from <0.1 to 336.6 ng $m^{-3,}$ respectively. In Atlantic TSP, d-Fe concentration was correlated with d-Al concentration, suggesting that the dissolved fractions of these metals were controlled by similar processes (Figure S5b). In contrast to the spatial distribution of T-Fe, the highest d-Fe concentrations were not observed in the coastal region near the Sahara Desert, but mainly between 20–30°W and 10–20°N (Figure 9b). This result suggests that, unlike North Pacific aerosols, d-Fe and d-Al concentrations in Atlantic aerosols were not controlled simply by mineral dust loading, as also reflected by the weak correlations of d-Fe with T-Fe and d-Al with T-Al (Figures S5c and S5d). The relatively low d-Fe concentrations in the coastal Saharan region likely reflect the dominance of freshly emitted mineral dust with low Fe_{sol}%. In contrast, the higher d-Fe concentrations observed around 20–30°W may indicate that mineral dust became more soluble during atmospheric transport through chemical alteration. Indeed, many samples were plotted in area (i), suggesting that mineral dust was solubilized through proton-promoted dissolution during atmospheric transport (Figure S4b). Atlantic aerosols showed a relatively large number of samples in area (v), where the influence of fly ash derived from high-temperature combustion is generally expected to be significant, compared with the other oceanic regions (Figure S4b). Considering that Saharan dust often exhibits [d-Fe]/[d-Al] ratios below 0.10, the samples plotted in area (v) likely reflect the contribution of Saharan dust with low [d-Fe]/[d-Al] ratios, rather than fly ash derived from high-temperature combustion. This interpretation is consistent with the near absence of samples in the area characterized by high-temperature combustion-derived $EF_{T\text{-}Fe}$ and anthro-Fe with high [d-Fe]/[d-Al] ratios. By contrast, aerosols with high $EF_{T\text{-}Fe}$ were mainly plotted in area (iii), indicating that anthro-Fe over the Atlantic was likely present mainly as insoluble Fe.

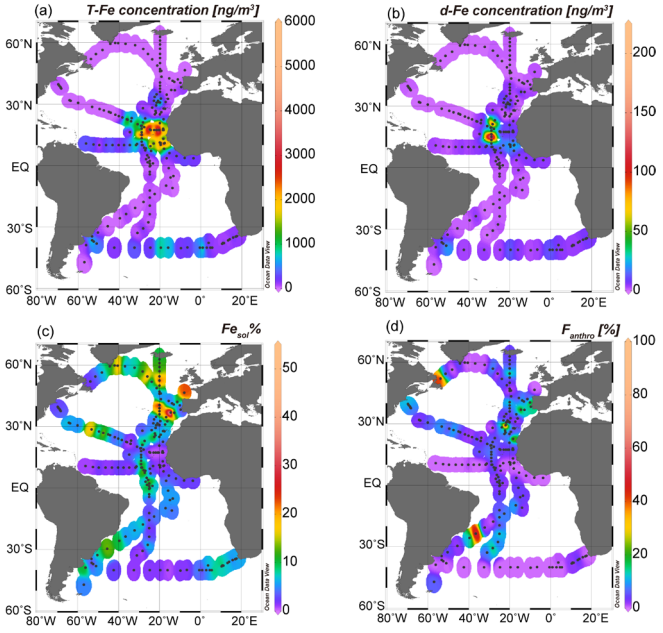

Figure 9. Spatial distributions of (a) T-Fe concentration, (b) d-Fe concentration, (c) Fe_{sol}%, and (d) $f_{anthro\text{-}dFe}$ in the Atlantic aerosols.

Unfortunately, Atlantic TSP samples collected from February to April are not available in this dataset. However, shipboard observations showed that T-Fe and T-Al concentrations were clearly higher in December–February than in June–August (Figure 10a). Considering the spatial variability in the sampling locations, the high concentrations observed in December–February likely mainly reflect the influence of the region offshore of the Sahara Desert. Indeed, similar seasonal variations in T-Fe concentrations have also been reported from ground-based observations at Cape Verde, located offshore of the Sahara Desert (Carpenter et al., 2010; Fomba et al., 2013; Patey et al., 2015). In contrast, satellite observations of DAOD over the same latitudinal region indicate a June–August peak, which is also consistent with the seasonal variability of dust deposition fluxes recorded by sediment traps in seawater (Yu et al., 2019; van der Does et al., 2021). This discrepancy is most likely explained by seasonal differences in the transport altitude of Saharan dust. During June-August, the northward shift of the Intertropical Convergence Zone (ITCZ) leads to the convergence of moist air from the south and dry air from the north between 15°N and 22°N, forming the Saharan Air Layer (SAL), which lifts mineral dust to altitudes of 5–7 km and transports it westward over the Atlantic Ocean (Adams et al., 2012; Muhs et al., 2013). In December to May, mineral dust is transported mainly in the lower troposphere and is therefore readily captured by shipboard and ground-based observations. As a result, DAOD and wet deposition to the ocean are enhanced in June-August, whereas the signal in near-surface observations becomes weaker (van der Does et al., 2021). Therefore, in the Atlantic Ocean, particularly in regions offshore of the Sahara, it may be difficult to comprehensively understand aerosol Fe supply processes based solely on shipboard and ground-based observations.

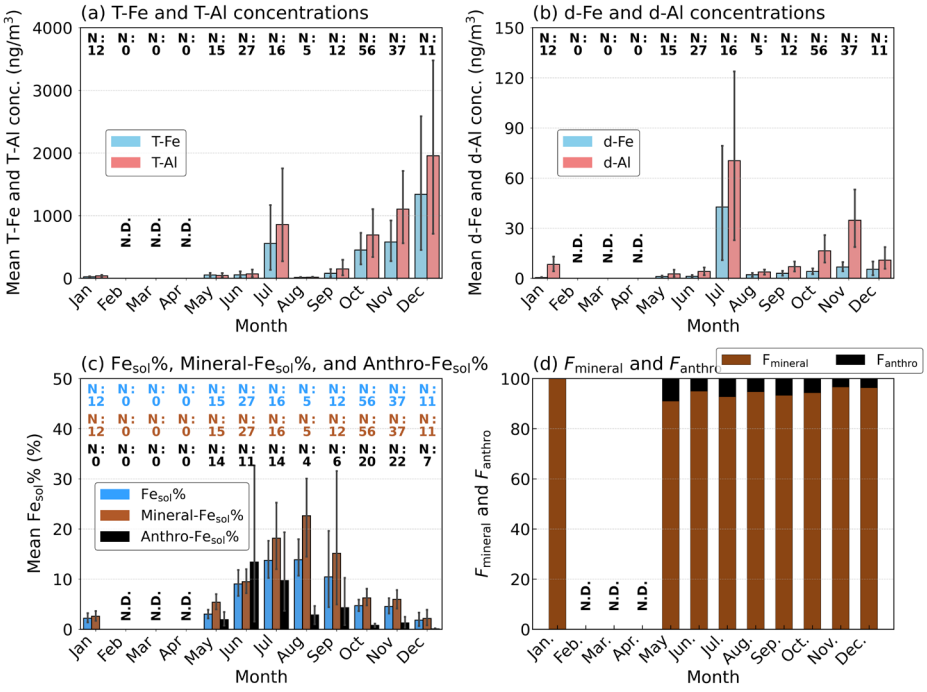

Figure 10. Monthly variations of (a) T-Fe and T-Al concentrations, (b) d-Fe and d-Al concentrations, (c) Fe_{sol}%, mineral-Fe_{sol}%, and anthro-Fe_{sol}%, and (d) $f_{mineral\text{-}dFe}$ and $f_{anthro\text{-}dFe}$ in the Atlantic aerosols.

3.4.2 The impact of anthro-Fe on Fe_{sol}%

The annual mean Fe_{sol}% of Atlantic TSPs was 6.2 ± 6.8% (range: 0.1–50.8%), and Fe_{sol}% tended to be higher in June-August (Figure 10c). High Fe_{sol}% values (>10%) were predominantly observed in the coastal regions of Europe and North America (Figure 9c). Previous studies have reported negative Fe isotope signatures attributable to combustion-derived anthro-Fe in these regions (Conway et al., 2019). However, comparison of Figures 9c and 9d shows that the locations of high Fe_{sol}% do not necessarily coincide with those of elevated $f_{anthro\text{-}dFe}$, suggesting that combustion-derived anthro-Fe is not a primary driver of the spatial variability in Fe_{sol}% over the Atlantic.

This interpretation is further supported by the source apportionment results for anthro-Fe. Most anthro-Fe in Atlantic aerosol samples was distributed below the boundary line separating non-combusted and combusted anthro-Fe, with a mean anthro-Fe_{sol}% of 1.0 ± 1.7% (Figure 11a). This indicates that anthro-Fe in Atlantic aerosols was dominated primarily by non-combustion-derived, low-solubility Fe. In contrast, samples influenced by relatively soluble combustion-derived anthro-Fe, represented by those plotted above the boundary line (mean anthro-Fe_{sol}%: 14.5 ± 22.2%), were less common than samples influenced by non-combustion-derived anthro-Fe (Figure 11a). A similar pattern was observed in both coarse and fine aerosol particles (Figures 11b and 11c). These results suggest that anthro-Fe contributed little to the direct increase in d-Fe or to the enhancement of bulk Fe_{sol}%. Therefore, the seasonal and spatial variability of Fe_{sol}% in Atlantic aerosols was more likely controlled by the aging state of mineral dust than by anthro-Fe input.

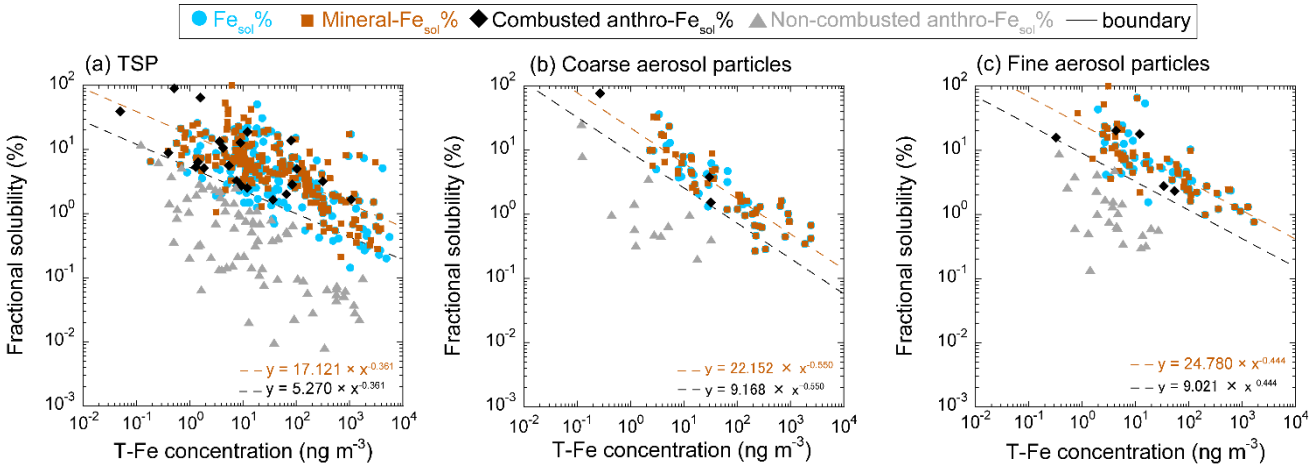

Figure 11. The inverse relationship of T-Fe, mineral-Fe, and anthro-Fe with their respective concentrations in (a) TSP, (b) coarse aerosol particles, and (c) fine aerosol particles collected in the Atlantic. Brown dashed lines indicate the power-law fits for mineral-Fe_{sol}%, whereas black dashed lines denote the boundaries separating combusted and non-combusted anthro-Fe.

3.4.3 The impact of chemical alteration on Fe_{sol}%

The monthly average Fe_{sol}% of Atlantic aerosols tended to be higher in June-August than in other seasons (Figure 10c). The same trend was found in the latitude band most affected by the Sahara Desert (Equator to 30°N). The East Asian region shows comparable seasonal variability in Fe_{sol}% (Figure 4a–4c), which has been attributed primarily to the temperature dependence of aerosol pH (Tao and Murphy, 2019b; Zhang et al., 2023; Yang and Weber, 2022). In contrast, the Sahara-affected latitude band (Equator to 30°N) experiences relatively minor annual temperature effects, suggesting that other factors contribute to the observed seasonal variability of Fe_{sol}%.

A likely explanation is the seasonal difference in the transport altitude and atmospheric processing of Saharan dust. In December-February, mineral dust is transported mainly below 3 km. Because there are no heavily polluted regions between the Sahara Desert and the Atlantic Ocean, the dust is not strongly aged by atmospheric pollutants such as sulfate and nitrate (Fitzgerald et al., 2015). Furthermore, relatively low precipitation in December-February likely suppresses wet deposition and chemical alteration in cloud water. Consequently, Atlantic aerosol samples collected near the surface in December-February exhibited higher Fe concentrations but lower Fe_{sol}%. During June-August, by contrast, mineral dust is predominantly transported above 3 km, where precipitation is higher. In particular, the increase in precipitation from August to October (Varela-Lopes and Molion, 2014) likely promotes the incorporation of mineral dust into cloud water, where aqueous-phase reactions driven by proton-promoted and ligand-promoted dissolution may enhance Fe_{sol}%. However, under the moderately acidic conditions of Atlantic cloud water (pH > 4.0; Shah et al., 2020), Fe dissolution is not expected to be as substantial as in more acidic regions, even in the presence of organic ligands (Bibi et al., 2011; Paris et al., 2011; Paris and Desboeufs, 2013; Bray et al., 2015). Observations using aerosol time-of-flight mass spectrometry also confirmed that mineral dust over the Atlantic undergoes chemical alteration by oxalate in cloud water (Fitzgerald et al., 2015). Thus, June-August cloud-water processing likely enhances Fe_{sol}% in Atlantic aerosols, but not to the extent observed in the North Pacific, where aerosol acidity is often much stronger, as reflected by the lower mean Fe_{sol}% of Atlantic aerosols (5.9%) than of North Pacific aerosols (15.1%).

3.5 The South Pacific Ocean

The T-Fe and T-Al concentrations in South Pacific TSPs ranged from 0.1 to 129.8 ng m^{-3} and 0.2 to 207.2 ng m^{-3}, respectively, with the highest values observed in coastal regions (Figure 12a). T-Fe was strongly correlated with T-Al (slope = 0.92), and the mean $EF_{T\text{-}Fe}$ was 1.9 ± 1.4 (range: 0.1–7.6). The $EF_{T\text{-}Fe}$ in the South Pacific TSPs was slightly higher than in North Pacific and Atlantic TSPs but still close to unity. $EF_{T\text{-}Fe}$ tended to be elevated in the marine area southwest of Australia, especially around Heard Island (Figure S6), likely reflecting the influence of volcanic bedrock on the island (Perron et al., 2021). Overall, however, T-Fe in South Pacific TSPs was derived mainly from mineral dust.

The concentrations of d-Fe and d-Al ranged from <0.1 to 8.3 ng m^{-3} and <0.1 to 12.6 ng m^{-3}, respectively, and showed a strong correlation (r = 0.77). Fe_{sol}% ranged from <0.1 to 100% (mean: 8.5 ± 12.5%); excluding one sample with Fe_{sol}% of

100%, the maximum was 41.9% and the mean was 7.3 ± 6.4%. The mean [d-Fe]/[d-Al] ratio in South Pacific TSPs was 0.73 ± 1.30, higher than those in North Pacific and Atlantic TSPs (0.39 ± 0.29 and 0.25 ± 0.48, respectively). High $f_{anthro\text{-}dFe}$ values, characterized by elevated [d-Fe]/[d-Al], were mainly detected near Heard Island, where $EF_{T\text{-}Fe}$ was also high (Figure S6). Given the basaltic volcanic rocks on Heard Island, this enrichment is more plausibly explained by volcanic source composition than by enhanced anthropogenic input (Perron et al., 2021).

TSP samples with Fe_{sol}% exceeding 10% were mainly observed along the Australian coast (Figure 12c). Previous studies reported that elevated Fe_{sol}% on the southeastern coast reflects anthro-Fe from urban areas together with aerosol acidification driven by anthropogenic SO_2 and NOx (Perron et al., 2020a). Consistent with this interpretation, our [d-Fe]/[d-Al] analysis suggests that up to ~20% of d-Fe in this region was derived from anthro-Fe. In northern and northeastern Australia, high Fe_{sol}% has also been linked to biomass burning (Perron et al., 2020a). However, previous studies suggest that Fe associated with biomass burning mainly reflects resuspended dry soil rather than direct Fe emission (Andreae et al., 2001; Kurisu and Takahashi, 2019), and observations at Gun Point indicate that the elevated Fe_{sol}% is driven not by direct d-Fe emission but by chemical interactions between Fe and organic matter emitted during fires (Winton et al., 2016). Consistent with this, TSP samples from northeastern Australia showed [d-Fe]/[d-Al] ratios above 1.0 despite $EF_{T\text{-}Fe}$ values below 2.0 (Figure S6), a pattern consistent with ligand-promoted dissolution of mineral dust. High $f_{anthro\text{-}dFe}$ values were also observed in southeastern Australia (Figure 12d), where volcanic rocks with high T-Fe/T-Al ratios have been reported. This suggests that the elevated [d-Fe]/[d-Al] ratio in this region may likewise reflect source-composition effects rather than anthropogenic input, although further investigation is needed.

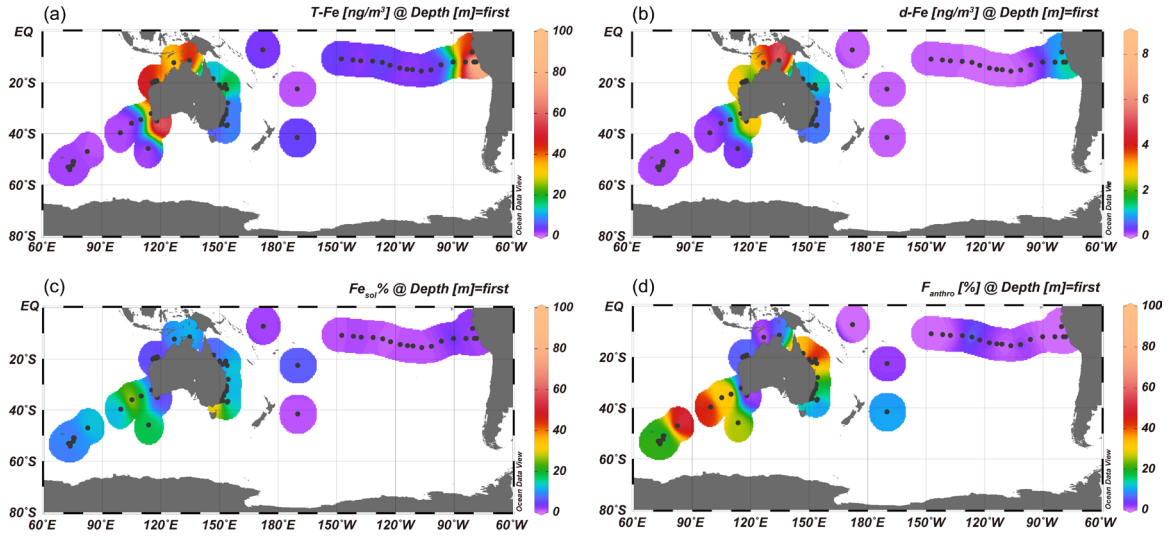

Figure 12. Spatial distribution of (a) T-Fe concentration, (b) d-Fe concentration, (c) Fe_{sol}%, and (d) $f_{anthro\text{-}dFe}$ in the South Pacific aerosols.

4. Implications

The factors controlling Fe_{sol}% in aerosol particles were investigated by compiling data for total and dissolved Fe and Al in aerosol particles. An inverse relationship between total Fe and Fe_{sol}% was observed, as has been reported in previous studies (Sholkovitz et al., 2009; Mahowald et al., 2018). When similar plots were constructed separately for mineral-Fe and anthro-Fe, inverse relationships between concentration and solubility were found for both components. The inverse relationship for mineral-Fe is likely explained by chemical alteration during atmospheric transport, because freshly emitted or unaged mineral particles generally have low Fe_{sol}%. In contrast, the anthro-Fe results indicated more diverse behavior. In samples with comparable anthro-Fe and mineral-Fe concentrations, two major groups were identified: one in which anthro-Fe_{sol}% was lower than mineral-Fe_{sol}%, and another in which anthro-Fe_{sol}% was comparable to mineral-Fe_{sol}%. The former group was mainly found in coarse aerosol particles collected in East Asia and showed extremely low anthro-Fe_{sol}% (<0.1%), suggesting contributions from brake-pad wear from vehicles and related sources. The latter group was mainly found in fine aerosol particles and showed a high average anthro-Fe_{sol}% of 22.2 ± 24.0%. Although anthro-Fe in fine particles is generally associated with high-temperature combustion processes, only a limited number of samples had anthro-Fe_{sol}% higher than that reported for highly soluble emissions such as heavy oil combustion (>37.0%). This suggests that a part of the anthro-Fe emitted with initially low solubility from solid fuel combustion, including coal combustion and the steel industry, was solubilized during atmospheric transport. Similar inverse relationships between concentrations and solubilities for mineral-Fe and anthro-Fe were also observed in marine aerosol particles. Therefore, inverse-correlation plots for mineral-Fe and anthro-Fe may provide a useful approach for evaluating source-dependent variations in Fe_{sol}% and for distinguishing anthro-Fe derived from high-temperature combustion from that derived from non-high-temperature combustion sources.

This study also estimated $f_{anthro\text{-}dFe}$ in marine aerosol particles based on the [d-Fe]/[d-Al] ratio. As a result, the contribution of anthro-Fe to d-Fe in the marine TSP samples was not large (North Pacific: 6.1 ± 10.4, Atlantic: 5.1 ± 9.7%). Although high $f_{anthro\text{-}dFe}$ was occasionally found in North Pacific TSPs influenced by ship emissions, $f_{anthro\text{-}dFe}$ in the open ocean was lower than coastal regions. Complementing our findings, Fe isotope analysis of d-Fe in marine aerosols consistently indicates large and small anthropogenic contributions to d-Fe in coastal and in the open oceans, respectively (Labatut et al., 2014; Conway et al., 2019; Kurisu et al., 2021, 2024). In contrast to these observational results, modeling studies have indicated substantial anthropogenic contributions to d-Fe, with $f_{anthro\text{-}dFe}$ exceeding 20% (Scanza et al., 2018; Hamilton et al., 2019; Rathod et al., 2020, 2024; Ito et al., 2021; Ito and Miyakawa, 2023). The discrepancy in $f_{anthro\text{-}dFe}$ between models and observations may be partly explained by the lower mineral-Fe_{sol}% represented in the models compared with values derived from field observations. Representative model calculations generally predict mineral-Fesol% of less than 10% for fine aerosol particles over the North Pacific. In contrast, mineral-Fe_{sol}% in fine aerosol particles frequently exceeded 10% in this study, with mean values of 28.5 ± 28.7% in the North Pacific and 11.3 ± 16.7% in the Atlantic. Thus, underestimation of mineral-Fe_{sol}% in fine particles may lead to an underestimation of mineral-derived d-Fe and, consequently, an overestimation of the relative contribution of anthro-Fe to total d-Fe. Incorporating a size-dependent scheme capable of representing higher mineral-Fe_{sol}% in fine particles may

therefore improve the representation of atmospheric Fe supply to the surface ocean and its source apportionment in Earth system models.

To better understand the sources of d-Fe in marine aerosols and their chemical alteration processes, observational studies, focusing on the [d-Fe]/[d-Al] ratio and Fe isotope ratios, are essential. These studies help us grasp the factors influencing $f_{anthro\text{-}dFe}$, $f_{mineral\text{-}dFe}$, mineral-Fe_{sol}%, and anthro-Fe_{sol}% variability. While representative values for mineral dust are established for both [d-Fe]/[d-Al] and Fe isotope ratios, large uncertainties persist regarding representative values for anthro-Fe and the variability among different emission sources. Constructing a robust database of [d-Fe]/[d-Al] and Fe isotope ratios for individual anthropogenic emission sources (e.g., coal combustion, steel industry, biomass burning, and non-combusted anthro-Fe) is crucial because the representative values of [d-Fe]/[d-Al] and Fe isotope ratios for anthro-Fe affect the calculation results of $f_{mineral\text{-}dFe}$ and $f_{anthro\text{-}dFe}$.

Code and data availability

Data archiving is underway in Zenodo, and the dataset will be made publicly available via Zenodo upon acceptance (doi: 10.5281/zenodo.19186414).

Supplement link

The link to the supplement will be included by Copernicus, if applicable.

Author contributions

KS and YT designed this study. KS and MK compiled dataset using this study. KS developed the model and performed the simulations. KS prepared the manuscript with contributions from all co-authors.

Competing interests

The authors declare that they have no conflict of interest.

Acknowledgements

The International GEOTRACES program is possible in part thanks to the support from the U.S. National Science Foundation (Grant OCE-2140395) to the Scientific Committee on Oceanic Research (SCOR). This paper also contributes to the science plan of the Surface Ocean-Lower Atmosphere Study (SOLAS), which is partially supported by the U.S. National Science Foundation (Grant OCE-1840868) via the Scientific Committee on Oceanic Research (SCOR).

Review statement

The review statement will be added by Copernicus Publications listing the handling editor as well as all contributing referees according to their status anonymous or identified.

References

Adams, A. M., Prospero, J. M., Zhang, C.: CALIPSO-derived three-dimensional structure of aerosol over the Atlantic basin and adjacent continents, J. Clim., 25, 6862–6879, https://doi.org/10.1175/JCLI-D-11-00672.1, 2012.

Andreae, M. O., Fischer, A. H., Freitas, S. R., Grégoire, J. M., Hoor, H. P., Kormann, R., Krejci, R., Lange, L., Lelieveld, J., Lindinger, W., Longo, K., Peters, W., de Reus, M., Scheeren, B., Silva, M. A. F., Ström, J., van Velthoven, P. F. J., Williams, J.: Transport of biomass burning smoke to the upper troposphere by deep convection in the equatorial region, Geophys. Res. Lett., 28, 951–954, https://doi.org/10.1029/2000GL012391, 2001.

Baker, A. R., Adams, C., Bell, T. G., Jickells, T. D., Ganzeveld, L.: Estimation of atmospheric nutrient inputs to the Atlantic Ocean from 50°N to 50°S based on large-scale field sampling: Iron and other dust-associated elements, Global Biogeochem. Cycles, 27, 755–767, https://doi.org/10.1002/gbc.20062, 2013.

Baker, A. R., Croot, P. L.: Atmospheric and marine controls on aerosol iron solubility in seawater, Mar. Chem., 120, 4–13, https://doi.org/10.1016/j.marchem.2008.09.003, 2010.

Baker, A. R., French, M., Linge, K. L.: Trends in aerosol nutrient solubility along a west–east transect of the Saharan dust plume, Geophys. Res. Lett., 33, L07805, https://doi.org/10.1029/2005GL024764, 2006a.

Baker, A. R., Jickells, T. D., Witt, M., Linge, K. L.: Trends in the solubility of iron, aluminium, manganese and phosphorus in aerosol collected over the Atlantic Ocean, Mar. Chem., 98, 43–58, https://doi.org/10.1016/j.marchem.2005.06.004, 2006b.

Baker, A. R., Kanakidou, M., Nenes, A., Myriokefalitakis, S., Croot, P. L., Duce, R. A., Gao, Y., Guieu, C., Ito, A., Jickells, T. D., Mahowald, N. M., Middag, R., Perron, M. M. G., Sarin, M. M., Shelley, R., and Turner, D. R.: Changing atmospheric acidity as a modulator of nutrient deposition and ocean biogeochemistry, Sci. Adv., 7, eabd8800, https://doi.org/10.1126/sciadv.abd8800, 2021.

Baker, A. R., Li, M., Chance, R.: Trace metal fractional solubility in size-segregated aerosols from the tropical eastern Atlantic Ocean, Global Biogeochem. Cycles, 34, e2019GB006510, https://doi.org/10.1029/2019GB006510, 2020.

Bibi, I., Singh, B., Silvester, E.: Dissolution of illite in saline–acidic solutions at 25°C, Geochim. Cosmochim. Acta, 75, 3237–3249, https://doi.org/10.1016/j.gca.2011.03.022, 2011.

Boyd, P. W., Jickells, T., Law, C. S., Blain, S., Boyle, E. A., Buesseler, K. O.: Mesoscale iron enrichment experiments 1993–2005: Synthesis, and future directions, Science, 315, 612–617, https://doi.org/10.1126/science.1131669, 2007.

Bray, A. W., Oelkers, E. H., Bonneville, S., Wolff-Boenisch, D., Potts, N. J., Fones, G., Benning, L. G.: The effect of pH, grain size, and organic ligands on biotite weathering rates, Geochim. Cosmochim. Acta, 164, 127–145, https://doi.org/10.1016/j.gca.2015.04.048, 2015.

Buck, C. S., Landing, W. M., Resing, J. A., Lebon, G. T.: Aerosol iron and aluminum solubility in the northwest Pacific Ocean: Results from the 2002 IOC cruise, Geochem. Geophys. Geosyst., 7, Q04M07, https://doi.org/10.1029/2005GC000977, 2006.

Buck, C. S., Landing, W. M., Resing, J. A., Measures, C. I.: The solubility and deposition of aerosol Fe and other trace elements in the North Atlantic Ocean: Observations from the A16N CLIVAR/CO2 repeat hydrography section, Mar. Chem., 120, 57–70, https://doi.org/10.1016/j.marchem.2008.08.003, 2010a.

Buck, C. S., Landing, W. M., Resing, J. A.: Particle size and aerosol iron solubility: A high-resolution analysis of Atlantic aerosols, Mar. Chem., 120, 14–24, https://doi.org/10.1016/j.marchem.2008.11.002, 2010b.

Buck, C. S., Landing, W. M., Resing.: , J. A.: Pacific Ocean aerosols: Deposition and solubility of iron, aluminum, and other trace elements, Mar. Chem., 157, 117–130, https://doi.org/10.1016/j.marchem.2013.09.005, 2013.

Buck, C. S., Paytan, A.: Evaluation of commonly used filter substates for the measurement of aerosol trace element solubility, Limnol Oceanogr Methods, 10, 790–806, https://doi.org/10.4319/lom.2012.10.790, 2012.

Buck, C.S., Aguilar-Islas, A., Marsay, C., Kadko, D., Landing, W. M.: Trace element concentrations, elemental ratios, and enrichment factors observed in aerosol samples collected during the US GEOTRACES eastern Pacific Ocean transect (GP16), Chem. Geol., 511, 212–224, https://doi.org/10.1016/j.chemgeo.2019.01.002, 2019.

Carpenter, L. J., Fleming, Z. L., Read, K. A., Lee, J. D., Moller, S. J., Hopkins, J. R., Purvis, R. M., Lewis, A. C., Müller, K., Heinold, B., Herrmann, H., Fomba, K. W., van Pinxteren, D., Müller, C., Tegen, I., Wiedensohler, A., Müller, T., Niedermeier, N., Achterberg, E. P., Patey, M. D., Kozlova, E. A., Manning, A. J., and Wallace, D. W. R.: Seasonal characteristics of tropical marine boundary layer air measured at the Cape Verde Atmospheric Observatory, J. Atmos. Chem., 67, 87–140, https://doi.org/10.1007/s10874-011-9206-1, 2011.

Chance, R., Jickells, T. D., Baker, A. R.: Atmospheric trace metal concentrations, solubility and deposition fluxes in remote marine air over the south-east Atlantic, Mar. Chem., 177, 45–56, https://doi.org/10.1016/j.marchem.2015.06.028, 2015.

Chang, C. Y., Wang, C. F., Mui, D. T., and Chiang, H. L.: Application of methods (sequential extraction procedures and high-pressure digestion method) to fly ash particles to determine the element constituents: A case study for BCR-176. J. Hazard. Mater., 163, 578–587, https://doi.org/10.1016/j.jhazmat.2008.07.039, 2009.

Chao, T. T., Sanzolone, R. F.: Decomposition techniques, J. Geochem. Explor., 44, 65–106, https://doi.org/10.1016/0375-6742(92)90048-D, 1992.

Charlson, R. J., Lovelock, J. E., Andreae, M. O., Warren, S. G.: Oceanic phytoplankton, atmospheric sulphur, cloud albedo and climate, Nature, 326, 655–661, https://doi.org/10.1038/326655a0, 1987.

Cheize, M., Sarthou, G., Croot, P. L., Bucciarelli, E., Baudoux, A. C., and Baker, A. R.: Iron organic speciation determination in rainwater using cathodic stripping voltammetry, Anal. Chim., Acta, 736, http://dx.doi.org/10.1016/j.aca.2012.05.011, 45–54, 2012.

Chen, Y. Z., Zhang, T. Y., Wang, Z. Y., Zhu, Z. M., Zhang, Y. F., Liu, M. Y., Wang, F., Ren, Y., Shi, G. L., Zhang, G. H., Wang, X. M., and Tang, M. J.: Sources of total and dissolved aerosol iron at Xi'an, Northwest China: implications for solubility of aerosol iron from different sources, J. Environ. Sci., 165, 29-37, https://doi.org/10.1016/j.jes.2025.06.066, 2026.

Clough, R., Lohan, M. C., Ussher, S. J., Nimmo, M., Worsfold, P. J.: Uncertainty associated with the leaching of aerosol filters for the determination of metals in aerosol particulate matter using collision/reaction cell ICP-MS detection, Talanta, 208, 120377, https://doi.org/10.1016/j.talanta.2019.02.067, 2020.

Conway, T. M., Hamiliton, D. S., Shelley, R. U., Aguilar-Islas, A. M., Landing, W. M., Mahowald, N. M., John, S. G.: Tracing and constraining anthropogenic aerosol iron fluxes to the North Atlantic Ocean using iron isotopes, Nat. Commun., 10, 2628, https://doi.org/10.1038/s41467-019-10457-w, 2019.

Cui, W., Song, X., Su, Y., Chen, X., Wu, D., Li, Q.: Soluble iron in source-based anthropogenic $PM_{2.5}$ predominantly from steel industry and residential combustion in China, Geophys. Res. Lett., 52, e2025GL118603, https://doi.org/10.1029/2025GL118603, 2025.

Desboeufs, K. V., Losno, R., Colin, J. L.: Factors influencing aerosol solubility during cloud processes, Atmos. Environ., 35, 3529–3537, https://doi.org/10.1016/S1352-2310(00)00472-6, 2001.

Desboeufs, K., Formenti, P., Torres-Sánchez, R., Schepanski, K., Chaboureau, J.-P., Andersen, H., Cermak, J., Feuerstein, S., Laurent, B., Klopper, D., Namwoonde, A., Cazaunau, M., Chevaillier, S., Feron, A., Mirande-Bret, C., Triquet, S., and Piketh, S. J.: Fractional solubility of iron in mineral dust aerosols over coastal Namibia: a link to marine biogenic emissions?, Atmos. Chem. Phys., 24, 1525–1541, https://doi.org/10.5194/acp-24-1525-2024, 2024.

Duvall, R. M., Majestic, B. J., Shafer, M. M., Chuang, P. Y., Simoneit, B. R. T., Schauer, J. J.: The water-soluble fraction of carbon, sulfur, and crustal elements in Asian aerosols and Asian soils, Atmos. Environ., 42, 5872–5884, https://doi.org/10.1016/j.atmosenv.2008.03.028, 2008.

Fairlie, T. D., Jacob, D. J., Dibb, J. E., Alexander, B., Avery, M. A., van Deonklelaar, A., Zhang, L.: Impact of mineral dust on nitrate, sulfate, and ozone in transpacific Asian pollution plumes, Atmos. Chem. Phys., 10, 3999–4012, https://doi.org/10.5194/acp-10-3999-2010, 2010.

Fitzgerald, E., Ault, A. P., Zauscher, M. D., Mayol-Bracero, O. L., Prather, K. A.: Comparison of the mixing state of long-range transported Asian and African mineral dust, Atmos. Environ., 115, 19–25, https://doi.org/10.1016/j.atmosenv.2015.04.031, 2015.

Fomba, K. W., Müller, K., van Pinxteren, D., Herrmann, H.: Aerosol size-resolved trace metal composition in remote northern tropical Atlantic marine environment: case study Cape Verde islands, Atmos. Chem. Phys., 13, 4801–4814, https://doi.org/10.5194/acp-13-4801-2013, 2013.

Gitari, W. M., Fatoba, O. O., Petrik, L. F., and Vadapalli, V. R. K.: Leaching characteristics of selected south African fly ashes: Effect of pH on the release of major and trace species, J. Environ. Sci. Health A, 44, 206–220, https://doi.org/10.1080/10934520802539897, 2009.

Guo, H., Nenes, A., Weber, R. J.: The underappreciated role of nonvolatile cations in aerosol ammonium-sulfate molar ratios, Atmos. Chem. Phys., 18, 173407–17323, https://doi.org/10.5194/acp-18-17307-2018, 2018.

Guo, H., Sullivan, A. P., Campuzano-Jost, P., Schroder, J. C., Lopez-Hilfiker, F. D., Dibb, J. E., Jimenez, J. L., Thornton, J. A., Brown, S. S., Nenes, A., and Weber, R. J.: Fine particle pH and the partitioning of nitric acid during winter in the northeastern United States, J. Geophys. Res. Atmos., 121, 10355–10376, https://doi.org/10.1002/2016JD025311, 2016.

Halle, L. L., Palmqvist, A., Kampmann, K., Jensen, A., Hansen, T., Khan, F. R.: Tire wear particle and leachate exposures from a pristine and road-worn tire to Hyalella azteca: Comparison of chemical content and biological effects, Aquat Toxicol, 232, 105769, https://doi.org/10.1016/j.aquatox.2021.105769, 2021.

Hamilton, D. S., Scanza, R. A., Feng, Y., Guinness, J., Kok, J. F., Li, L., Liu, X., Rathod, S. D., Wan, J. S., Wu, M., and Mahowald, N. M.: Improved methodologies for Earth system modelling of atmospheric soluble iron and observation comparisons using the Mechanism of Intermediate complexity for Modelling Iron (MIMI v1.0), Geosci. Model Dev., 12, 3835–3862, https://doi.org/10.5194/gmd-12-3835-2019, 2019.

Harrison, R. M., Jones, A. M., Gietl, J., Yin, J., Green, D. C.: Estimation of the contributions of brake dust, tire wear, and resuspension to nonexhaust traffic particles derived from atmospheric measurements, Environ. Sci. Technol., 2012, 46, 6523–6529, https://doi.org/10.1021/es300894r, 2012.

Hsieh, C. C., You, C. F., Ho, T. Y.: The solubility and deposition flux of East Asian aerosol metals in the East China Sea: The effects of aeolian transport processes, Mar. Chem., 253, 104268, https://doi.org/10.1016/j.marchem.2023.104268, 2023.

Huang, S. J., Chang, C. Y., Mui, D. T., Chang, F. C., Lee, M. Y., and Wang, C. F.: Sequential extraction for evaluating the leaching behavior of selected elements in municipal solid waste incineration fly ash. J. Hazard. Mater., 149, 180–188, https://doi.org/10.1016/j.jhazmat.2007.03.067, 2007.

Ito, A. and Miyakawa, T.: Aerosol iron from metal production as a secondary source of bioaccessible iron, Environ. Sci. Technol., 57, 4091–4100, https://doi.org/10.1021/acs.est.2c06472, 2023.

Ito, A. Feng, Y.: Role of dust alkalinity in acid mobilization of iron, Atmos. Chem. Phys., 10, 9237–9250, https://doi.org/10.5194/acp-10-9237-2010, 2010.

Ito, A., Myriokefalitakis, S., Kanakidou, M., Mahowald, N. M., Scanza, R. A., Hamilton, D. S., Baker, A. R., Jickells, T. D., Sarin, M. M., Bikkina, S., Gao, Y., Shelley, R. U., Buck, C. S., Landing, W. M., Bowie, A. R., Perron, M. M. G., Guieu, C., Meskhidze, N., Johnson, M. S., Feng, Y., Kok, J. F., Nenes, A., and Duce, R. A.: Pyrogenic iron: The missing link to high iron solubility in aerosols, Sci. Adv., 5, eaau7671, https://doi.org/10.1126/sciadv.aau7671, 2019.

Ito, A., Ye, Y., Baldo, C., Shi, Z.: Ocean fertilization by pyrogenic aerosol iron, npj Clim. Atmos. Sci., 4, 30, https://doi.org/10.1038/s41612-021-00185-8, 2021.

Ito, A.: Global modeling study of potentially bioavailable iron input from shipboard aerosol sources to the ocean, Global Biogeochem. Cycles, 27, 1–10, https://doi.org/10.1029/2012GB004378, 2013.

Jickells, T. D., An, Z. S., Andersen, K. K., Baker, A. R., Bergametti, G., Brooks, N., Cao, J. J., Boyd, P. W., Duce, R. A., Hunter, K. A., Kawahata, H., Kubilay, N., LaRoche, J., Liss, P. S., Mahowald, N. M., Prospero, J. M., Ridgwell, A. J., Tegen, I., and Torres, R.: Global iron connections between desert dust, ocean biogeochemistry, and climate, Science, 308, 67–71, https://doi.org/10.1126/science.1105959, 2005.

Jin, X., Frenzel, G. H., Doney, S. C., McWilliams, J. C.: The impact of atmospheric CO_2 of iron fertilization induced changes in the ocean's biological pump, Biogeosci., 5, 385–406, https://doi.org/10.5194/bg-5-385-2008, 2008.

Journet, E., Desboeufs, K. V., Caquineau, S., Colin, J. L.: Mineralogy as a critical factor of dust iron solubility, Geophys. Res. Lett., 35, L07805, https://doi.org/10.1029/2007GL031589, 2008.

Kajino, M., Hagino, H., Fujitani, Y., Morikawa, T., Fukui, T., Onishi, K., Okuda, T., Kajikawa, T., Igarashi, Y.: Modeling transition metals in East Asia and Japan and its emission sources, GeoHealth, 4, e2020GH000259, https://doi.org/10.1029/2020GH000259, 2020.

Kanakidou, M., Myriokefalitakis, S., Tsigaridis, K.: Aerosols in atmospheric chemistry and biogeochemical cycles of nutrients, Environ. Res. Lett., 13, 063004, https://doi.org/10.1088/1748-9326/aabcdb, 2018.

Kawai, K., Matsui, H., Tobo, Y.: High potential of Asian dust to act as ice nucleating particles in mixed-phase clouds simulated with a global aerosol-climate model, J. Geophys. Res. Atmos., 126, e2020JD034263, https://doi.org/10.1029/2020JD034263, 2021.

Kieber, R. J., Willey, J. D., Broooks Avery Jr., G.: Temporal variability of rainwater iron speciation at the Bermuda Atlantic Time Series Station, J. Geophys. Res. Ocean, 108, 3277, https://doi.org/10.1029/2001JC001031, 2003.

Kim, A. G., Kazonich, G., and Dahlberg, M.: Relative solubility of cations in class F fly ash, Environ. Sci. Technol., 37, 4507–4511, https://doi.org/10.1021/es0263691, 2003.

Kodama, H., and Schnitzer, M.: Dissolution of chlorite minerals by fulvic acid, Can. J. Soil Sci., 53, 240–243, https://doi.org/10.4141/cjss73-036, 1973.

Komonweeraket, K., Cetin, B., Aydilek, A. H., Benson, C. H., and Edil, T. B.: Effects of pH on the leaching mechanisms of elements from fly ash mixed soils, Fuel, 140, 788–802, http://dx.doi.org/10.1016/j.fuel.2014.09.068, 2015.

Krishnamurthy, A., Moore, J. K., Mahowald, N., Luo, C., Doney, S., Linday, K., Zender, C. S.: Impacts of increasing anthropogenic soluble iron and nitrogen deposition on ocean biogeochemistry, Global Biogeochem. Cycles, 23, GB3016, https://doi.org/10.1029/2008GB003440, 2009.

Kurisu, M., Adachi, K., Sakata, K., Takahashi, Y.: Stable isotope ratios of combustion iron produced by evaporation in a steel plant, ACS Earth Space Chem.,. 3, 588–598, https://doi.org/10.1021/acsearthspacechem.8b00171, 2019.

Kurisu, M., Sakata, K., Nishioka, J., Obata, H., Conway, T. M., Hunt, H. R., Sieber, M., Suzuki, K., Kashiwabara, T., Kubo, S., Takada, M., and Takahashi, Y.: Source and fate of atmospheric iron supplied to the subarctic North Pacific traced by stable iron isotope ratios, Geochim. Cosmochim. Acta, 378, 168–185, https://doi.org/10.1016/j.gca.2024.06.009, 2024.

Kurisu, M., Sakata, K., Uematsu, M., Ito, A., Takahashi, Y.: Contribution of combustion Fe in marine aerosols over the northwestern Pacific estimated by Fe stable isotope ratio, Atmos. Chem. Phys., 21, 16027–16050, https://doi.org/10.5194/acp-21-16027-2021, 2021.

Kurisu, M., Takahashi, Y.: Testing iron stable isotope ratios as signature of biomass burning, Atmos., 10, 76, https://doi.org/10.3390/atmos10020076, 2019.

Kurisu, M., Zhu, C., Miyakawa, T., Ito, A., Suzuki, K., Kashiwabara, T.: Identification of anthropogenic Fe originated from East Asia using Fe stable isotope ratios of aerosols collected on Fukue Island, Atmos. Environ., 373, 121893, https://doi.org/10.1016/j.atmosenv.2026.121893, 2026.

Kurokawa, J., and Ohara, T.: Long-term historical trends in air pollutant emissions in Asia: Regional emission inventory in Asia (REAS) version 3, Atmos. Chem. Phys., 20, 12761–12793, https://doi.org/10.5194/acp-20-12761-2020, 2020.

Labatut, M., Lacan, F., Pradoux, C., Chmeleff, J., Radic, A., Murray, J. W., Poitrasson, F., Johansen, A. M., and Thil, F.: Iron sources and dissolved-particulate interactions in the seawater of the Western Equatorial Pacific, iron isotope perspectives, Global Biogeochem. Cycles, 28, 1044–1065, https://doi.org/10.1002/2014GB004928, 2014.

Li, T., Wang, Y., Li, W.J., Chen, J. M., Wang, T., Wang, W. X.: Concentrations and solubility of trace elements in fine particles at a mountain site, southern China: regional sources and cloud processing, Atmos. Chem. Phys., 15, 8987–9002, https://doi.org/10.5194/acp-15-8987-2015, 2015.

Li, W., Xu, L., Liu, X., Zhang, J., Lin, Y., Yao, X., Gao, H., Zhang, D., Chen, J., Wang, W., Harrison, R., Shao, L., Fu, P., Nenes, A., and Shi, Z.: Air pollution–aerosol interactions produce more bioavailable iron for ocean ecosystems, Sci. Adv., 3, e1601749, https://doi.org/10.1126/sciadv.1601749, 2017.

Liu, X., Turner, J. R.., Hand, J. L., Schichtel, B. A., Martin, R. V.: A global-scale mineral dust equation, J. Geophys. Res. Atmos., 127, e2022JD036937, 2022.

Lowson, R. T., Comarmond, J., Rajaratnam, G., and Brown, P. L.: The kinetics of the dissolution of chlorite as a function of pH and at 25ºC, Geochim. Cosmochim. Acta, 69, 1687–1699, https://doi.org/10.1016/j.gca.2004.09.028, 2005.

Luo, C., Wang, W., Sheng, L., Zhou, Y., Hu, Z., Qu, W., Li, X., and Hai, S.: Influence of polluted dust on chlorophyll-a concentration and particulate organic carbon in the subarctic North Pacific Ocean based on satellite observation and the WRF-Chem simulation, Atmos. Res., 236, 104812, https://doi.org/10.1016/j.atmosres.2019.104812, 2020.

Ma, Q., Cai, S., Wang, S., Zhao, B., Martin, R. V., Brauer, M., Cohen, A., Jiang, J., Zhou, W., Hao, J., Frostad, J., Forouzanfar, M. H., and Burnett, R. T.: Impacts of coal burning on ambient PM2.5 pollution in China, Atmos. Chem. Phys., 17, 4477–4491, https://doi.org/10.5194/acp-17-4477-2017, 2017.

Mahowald, N. M., Engelstaedter, S., Luo, C., Sealy, A., Artaxo, P., Benitez-Nelson, C., Bonnet, S., Chen, Y., Chuang, P. Y., Cohen, D. D., Dulac, F., Herut, B., Johansen, A. M., Kubilay, N., Losno, R., Maenhaut, W., Paytan, A., Prospero, J. M., Shank, L. M., and Siefert, R. L.: Atmospheric iron deposition: Global distribution, variability and human perturbations, Ann. Rev. Mar. Sci., 1, 245–278, https://doi.org/10.1146/annurev.marine.010908.163727, 2009.

Mahowald, N. M., Hamilton, D. S., Mackey, K. R. M., Moore, J. K., Baker, A. R., Scanza, R. A. and Zhang, Y.: Aerosol trace metal leaching and impacts on marine microorganisms, Nat. Commun., 9, 1–15, https://doi.org/10.1038/s41467-018-04970-7, 2018.

Marsay, C. M., Kadko, D., Landing, W. M., Buck, C.: Bulk aerosol trace element concentrations and deposition fluxes during the U.S, GEOTRACES GP15 Pacific meridional transect, Global Biogeochem. Cycles, 36, e2021GB007122, https://doi.org/10.1029/2021GB007122, 2022.

Martin, J. H., Coale, K. H., Johnson, K. S., Fitzwater, S. E., Gordon, R. M., Tanner, S. J., Hunter, C. N., Elrod, V. A., Nowicki, J. L., Coley, T. L., Barber, R. T., Lindley, S., Watson, A. J., Van Scoy, K., Law, C. S., Liddicoat, M. I., Ling, R., Stanton, T., Stockel, J., Collins, C., Anderson, A., Bidigare, R., Ondrusek, M., Latasa, J., Millero, F. J., Lee, K., Yao, W., Zhang, J.-Z., Friederich, G., Sakamoto, C., Chavez, F., Buck, K., Kolber, Z., Greene, R., Falkowski, P., Chisholm, S. W., Hoge, F., and Tindale, N. W.: Testing the iron hypothesis in ecosystems of the equatorial Pacific Ocean, Nature, 371, 123–129, https://doi.org/10.1038/371123a0, 1994.

Martin, J. H., Fitzwater, S. E.: Iron deficiency limits phytoplankton growth in the north-east Pacific subarctic, Nature, 331, 341–343, https://doi.org/10.1038/331341a0, 1988.

Martin, J. H.: Glacial-interglacial CO_2 change: The iron hypothesis, Paleoceanography, 5, 1–13, https://doi.org/10.1029/PA005i001p00001, 1990.

Maters, E. C., Delmelle, P., Bonneville, S.: Atmospheric processing of volcanic glass: Effects on iron solubility and redox speciation, Environ. Sci. Technol., 50, 5033–5040, https://doi.org/10.1021/acs.est.5b06281, 2016.

Meskhidze, N., Chameides, W. L., Nenes, A.: Dust and pollution: A recipe for enhanced ocean fertilization? J. Geophys. Res., 110, D03301, https://doi.org/10.1029/2004JD005082, 2005.

Mitra, A., Rimstidt, J. D.: Solubility and dissolution rate of silica in acid fluoride solutions, Geochim. Cosmochim. Acta, 73, 7045–7059, https://doi.org/10.1016/j.gca.2009.08.027, 2009.

Miyamoto, C., Sakata, K., Yamakawa, Y., Takahashi, Y.: Determination of calcium and sulfate species in aerosols associated with the conversion of its species through reaction processes in the atmosphere and its influence on cloud condensation nuclei activation, Atmos. Environ., 223, 117193, https://doi.org/10.1016/j.atmosenv.2019.117193, 2020.

Morton, P. L., Landing, W. M., Hsu, S. C., Milne, A., Aguilar-Islas, A. M., Baker, A. R. Methods for the sampling and analysis of marine aerosols: results from the 2008 GEOTRACES aerosol intercalibration experiment.: Limnol. Oceanogr. Methods, 11, 62–78, https://doi.org/10.4319/lom.2013.11.62, 2013.

Muhs, D. R.: The geologic records of dust in the Quaternary, Aeolian Res., 9, 3–48, https://doi.org/10.1016/j.aeolia.2012.08.001, 2013.

Oakes, M., Ingall, E. D., Lai, B., Shafer, M. M., Hays, M. D., Liu, Z. G., Russell, A. G., and Weber, R. J.: Iron solubility related to particle sulfur content in source emission and ambient fine particles, Environ. Sci. Technol., 46, 6637–6644, https://doi.org/10.1021/es300701c, 2012.

Olgun, N., Duggen, S., Croot, P. L., Delmelle, P., Dietze, H., Schacht, U.: Surface ocean iron fertilization: The role of airborne volcanic ash from subduction zone and hot spot volcanoes and related iron fluxes into the Pacific Ocean, Global Biogeochem. Cycles, 36, GB4001, https://doi.org/10.1029/2009GB003761, 2011.

Paris, R., Desboeufs, K. V., Journet, E.: Variability of dust iron solubility in atmospheric waters: Investigation of the role of oxalate organic complexation, Atmos. Environ., 45, 6510−6517, https://doi.org/10.1016/j.atmosenv.2011.08.068, 2011.

Paris, R., Desboeufs, K. V.: Effect of atmospheric organic complexation on iron-bearing dust solubility, Atmos. Chem. Phys., 13, 4895–4905, https://doi.org/10.5194/acp-13-4895-2013, 2013.

Patey, M. D., Achterberg, E. P., Rijkenberg, M. J., Pearce, R.: Aerosol time-series measurements over the tropical Northeast Atlantic Ocean: Dust sources, elemental composition and mineralogy, Mar. Chem., 174, 103–119, https://doi.org/10.1016/j.marchem.2015.06.004, 2015.

Perron, M. M. G., Proemse, B. C., Strzelec, M., Gault-Ringold, M., Boyd, P. W., Rodriguez, E. S., Paull, B., and Bowie, A. R.: Origin, transport and deposition of aerosol iron to Australian coastal waters, Atmos. Environ., 228, 117432, https://doi.org/10.1016/j.atmosenv.2020.117432, 2020a.

Perron, M. M. G., Proemse, B. C., Strzelec, M., Gault-Ringold, M., Bowie, A. R.: Atmospheric inputs of volcanic iron around Heard and McDonald Islands, Southern ocean, Environ. Sci. Atmos., 1, 508, https://doi.org/10.1039/D1EA00054C, 2021.

Perron, M. M. G., Strzelec, M., Gault-Ringold, M., Proemse, B. C., Boyd, P. W., Bowie, A. R.: Assessment of leaching protocols to determine the solubility of trace metals in aerosols, Talanta, 208, 120377, https://doi.org/10.1016/j.talanta.2019.120377, 2020b.

Praharaj, T., Powell, M. A., Hart, B. R., and Tripathy, S.: Leachability of elements from sub-bituminous coal fly ash from India. Environ. Int., 27, 609–615, https://doi.org/10.1016/S0160-4120(01)00118-0, 2002.

Pye, H. O. T., Nenes, A., Alexander, B., Ault, A. P., Barth, M. C., Clegg, S. L., Collett Jr., J. L., Fahey, K. M., Hennigan, C. J., Herrmann, H., Kanakidou, M., Kelly, J. T., Ku, I.-T., McNeill, V. F., Riemer, N., Schaefer, T., Shi, G., Tilgner, A., Walker, J. T., Wang, T., Weber, R., Xing, J., Zaveri, R. A., and Zuend, A.: The acidity of atmospheric particles and clouds, Atmos. Chem. Phys., 20, 4809–4888, https://doi.org/10.5194/acp-20-4809-2020, 2020.

Rathod, S. D., Hamilton, D. S., Mahowald, N. M., Klimont, Z., Vorbett, J. J., Bond, T. C.: A mineralogy-based anthropogenic combustion-iron emission inventory, J. Geophys. Res. Atmos., 125, e2019JD032114, https://doi.org/10.1029/2019JD032114, 2020.

Rathod, S. D., Hamilton, D. S., Nino, L. L., Kreidenweis, S. M., Bian, Q., Mahowald, N. M., Alastuey, A., Querol, X., Paytan, A., Artaxo, P., Herut, B., Gaston, C., Prospero, J., Chellam, S., Hueglin, C., Varrica, D., Dongarra, G., Cohen, D. D.,

Smichowski, P., Gomez, D., Lambert, F., Barraza, F., Bergametti, G., Rodríguez, S., Gonzalez-Ramos, Y., Hand, J., Kyllönen, K., Hakola, H., Chuang, P. Y., Hopke, P. K., Harrison, R. M., Martin, R. V., Walsh, B., Weagle, C., Maenhaut, W., Morera-Gómez, Y., Chen, Y. C., Pierce, J. R., and Bond, T. C.: Constraining present-day anthropogenic total iron emission using model and observations, J. Geophys. Res. Atmos., 129, e2023JD040332, https://doi.org/10.1029/2023JD040332, 2024.

Rudnick, R. L., Gao, S.: Composition of the continental crust.: Treatise on Geochemistry, 3, 1–64, 2003.

Sakata, K., Kurisu, M., Takeichi, Y., Sakaguchi, A., Tanimoto, H., Tamenori, Y., Matsuki, A., and Takahashi, Y.: Iron (Fe) speciation in size-fractionated aerosol particles in the Pacific Ocean: The role of organic complexation of Fe with humic-like substances in controlling Fe solubility, Atmos. Chem. Phys., 22, 9461–9482, https://doi.org/10.5194/acp-22-9461-2022, 2022.

Sakata, K., Kurisu, M., Tanimoto, H., Sakaguchi, A., Uematsu, M., Miyamoto, C., Takahashi, Y.: Custom-made PTFE filters for ultra-clean size-fractionated aerosol sampling for trace metals, Mar. Chem., 206, 100– 108, https://doi.org/10.1016/j.marchem.2018.09.009, 2018.

Sakata, K., Sakaguchi, A., Yamakawa, Y., Miyamoto, C., Kurisu, M., Takahashi, Y.: Measurement report: Stoichiometry of dissolved iron and aluminum as an indicator of the factors controlling the fractional solubility of aerosol iron – results of the annual observations of size-fractionated aerosol particles in Japan, Atmos. Chem. Phys., 23, 9815–9836, https://doi.org/10.5194/acp-23-9815-2023, 2023.

Sakata, K., Takano, S., Matsuki, A., Takeichi, Y., Tanimoto, H., Sakaguchi, A., Kurisu, M., and Takahashi, Y.: Atmospheric chemistry in East Asia determines the iron solubility of aerosol particles supplied to the North Pacific Ocean, Atmos. Chem. Phys., 25, 11087–11107, https://doi.org/10.5194/acp-25-11087-2025, 2025.

Scanza, R. A., Hamilton, D. S., Perez Garcia-Pando, C., Buck, C., Baker, A., and Mahowald, N. M.: Atmospheric processing of iron in mineral and combustion aerosols: development of an intermediate-complexity mechanism suitable for Earth system models, Atmos. Chem. Phys., 18, 14175–14196, https://doi.org/10.5194/acp-18-14175-2018, 2018.Adams, A. M., Prospero, J. M., Zhang, C.: CALIPSO-derived three-dimensional structure of aerosol over the Atlantic basin and adjacent continents, J. Clim., 25, 6862–6879, https://doi.org/10.1175/JCLI-D-11-00672.1, 2012.

Schroth, A. W., Crusius, J., Sholkovitz, E. R., Bostick, B. C.: Iron solubility driven by speciation in dust sources to the ocean, Nat. Geosci., 2, 337–340, https://doi.org/10.1038/ngeo501, 2009.

Sedwick, P. N., Sholkovitz, E. R., Church, T. M.: Impact of anthropogenic combustion emissions on the fractional solubility of aerosol iron: Evidence from the Sargasso Sea, Geochem. Geophys. Geosyst., 8, Q10Q06, https://doi.org/10.1029/2007GC001586, 2007.

Seidel, A., and Zimmels, Y.: Mechanism and kinetics of aluminium and iron leaching from coal fly ash by sulfuric acid. Chem. Eng. Sci., 53, 3535–3852, https://doi.org/10.1016/S0009-2509(98)00201-2, 1998.

Seo, H., Kim, G.: Anthropogenic iron invasion into the ocean: Results from the East Sea (Japan Sea), Environ. Sci. Technol., 57, 10745–10753, https://doi.org/10.1021/acs.est.3c01084, 2023.

Shah, V., Jacob. D. J., Moch, J. M., Wang, X., Zhai, S.: Global modeling of cloud water acidity precipitation acidity, and acid inputs to ecosystems, Atmos. Chem. Phys., 20, 12223–12245, https://doi.org/10.5194/acp-20-12223-2020, 2020.

Shelley, R. U., Landing, W. M., Ussher, S. J., Planquette, H., Sarthou, G.: Regional trends in the fractional solubility of Fe and other metals from North Atlantic aerosols (GEOTRACES cruises GA01 and GA03) following a two-stage leach, Biogeosci., 15, 2271–2288, https://doi.org/10.5194/bg-15-2271-2018, 2018.

Shi, Z. B., Woodhouse, M. T., Carslaw, K. S., Krom, M. D., Mann, G. W., Baker, A. R., Savov, I., Fones, G. R., Brooks, B., Drake, N., Jickells, T. D., and Benning, L. G.: Minor effect of physical size sorting on iron solubility of transported mineral dust, Atmos. Chem. Phys., 11, 8459–8469, https://doi.org/10.5194/acp-11-8459-2011, 2011a.

Shi, Z., Bonneville, S., Krom, M. D., Carslaw, K. S., Jickells, T. D., Baker, A. R., Benning, L. G.: Iron dissolution kinetics of mineral dust at low pH during simulated atmospheric processing, Atmos. Chem. Phys., 11, 995–1007, https://doi.org/10.5194/acp-11-995-2011, 2011b.

Shi, Z., Krom, M. D., Bonneville, S., Benning, L. G.: Atmospheric processing outside clouds increases soluble iron in mineral dust, Environ. Sci. Technol., 49, 1472–1477, https://doi.org/10.1021/es504623x, 2015.

Sholkovitz, E. R., Sedwick, P. N., Church, T. M., Baker, A. R., Powell, C. F.: Fractional solubility of aerosol iron: Synthesis of a global-scale data set, Geochim. Cosmochim. Acta, 89, 173–189, https://doi.org/10.1016/j.gca.2012.04.022, 2012.

Sholkovitz, E. R., Sedwick, P. N., Church, T. M.: Influence of anthropogenic combustion emissions on the deposition of soluble aerosol iron to the ocean: Empirical estimates for island sites in th4e North Atlantic, Geochim. Cosmochim. Acta, 73, 3981–4003, 2009.

Shupert, L. A., Ebbs, S. D., Lawrence, J., Gibson, D. J., Filip, P.: Dissolution of copper and iron from automotive brake pad wear debris enhances growth and accumulation by the invasive macrophyte Salvinia molesta Mitchell, Chemosphere, 92, 45–51, https://doi.org/10.1016/j.chemosphere.2013.03.002, 2013.

Song, Q., Osada, K.: Seasonal variation of aerosol acidity in Nagoya, Japan and factors affecting it, Atmos. Environ. X, 5, 100062, https://doi.org/10.1016/j.aeaoa.2020.100062, 2020.

Song, Q., Zhang, Z., Yu, H., Ginoux, P., Shen, J.: Global dust optical depth climatology derived from CALIOP and MODIS aerosol retrievals on decadal timescales: regional and interannual variability, Atmos. Chem. Phys., 21, 13369–13395, https://doi.org/10.5194/acp-21-13369-2021, 2021.

Sullivan, R. C., Guazzotti, S. A., Sodeman, D. A., Prather, K. A.: Direct observations of the atmospheric processing of Asian mineral dust, Atmos. Chem. Phys., 7, 1213–1236, https://doi.org/10.5194/acp-7-1213-2007, 2007.

Takahashi, Y., Furukawa, T., Kanai, Y., Uematsu, M., Zheng, G., Marcus, M. A.: Seasonal changes in Fe species and soluble Fe concentration in the atmosphere in the Northwest Pacific region based on the analysis of aerosols collected in Tsukuba, Japan, Atmos. Chem. Phys., 13, 7695–7710, https://doi.org/10.5194/acp-13-7695-2013, 2013.

Takahashi, Y., Higashi, M., Furukawa, T., Mitsunobu, S.: Change of iron species and iron solubility in Asian dust during the long-range transport from western China to Japan, Atmos. Chem. Phys., 11, 11237–11252, https://doi.org/10.5194/acp-11-11237-2011, 2011.

Takahashi, Y., Miyoshi, T., Higashi, M., Kamioka, H., Kanai, Y.: Neutralization of calcite in mineral aerosols by acidic sulfur species collected in China and Japan studied by Ca K-edge X-ray absorption near-edge structure, Environ. Sci. Technol., 43, 6535–6540, https://doi.org/10.1021/es9010256, 2009.

Tang, M., Perron, M. M. G., Baker, A. R., Li, R., Bowie, A. R., Buck, C. S., Kumar, A., Shelley, R., Ussher, S. J., Clough, R., Meyerink, S., Panda, P. P., Townsend, A. T., and Wyatt, N.: Measurement of soluble aerosol trace elements: inter-laboratory comparison of eight leaching protocols, Atmos. Meas. Tech., 18, 6125–6141, https://doi.org/10.5194/amt-18-6125-2025, 2025.

Tao, Y., Murphy, J. G.: The mechanisms responsible for the interactions among oxalate, pH, and Fe dissolution in $PM_{2.5}$, ACS Earth Space Chem., 3, 2259−2265, https://doi.org/10.1021/acsearthspacechem.9b00172, 2019b.

Tao, Y., Murphy, J. G.: The sensitivity of $PM_{2.5}$ acidity to meteorological parameters and chemical composition changes: 10-year records from six Canadian monitoring sites, Atmos. Chem. Phys., 19, 9309–9320, https://doi.org/10.5194/acp-19-9309-2019, 2019a.

Taylor, S. R., McLennan, S. M.: The geochemical evolution of the continental crust, Rev. Geophys., 33, 241–265, https://doi.org/10.1029/95RG00262, 1995.

Taylor, S. R.: Abundance of chemical elements in the continental crust: a new table.: Geochim. Cosmochim. Acta, 28, 1273–1285, https://doi.org/10.1016/0016-7037(64)90129-2, 1964.

Turekian, K. K., Wedepohl, K. H.: Distribution of the elements in some major units of the Earth's crust, Geological Society of American Bulletin, 72, 175–192, https://doi.org/10.1130/0016-7606(1961)72[175:DOTEIS]2.0.CO,2, 1961.

Uematsu, M., Duce, R. A., Prospero, J. M., Chen, L., Merrill, J. T., McDonald, R. L.: Transport of mineral aerosol from Asia over the North Pacific ocean, J. Geophys. Res., 88, 5342–5352, https://doi.org/10.1029/jc088ic09p05343, 1983.

van der Does, M., Brummer, G. J. A., Korte, L. F., Stuut, J. B. W.: Seasonality in Saharan dust across the Atlantic Ocean: From atmospheric transport to seafloor deposition, J. Geophys. Res. Atmos., 126, e2021JD034614, https://doi.org/10.1029/2021JD034614, 2021.

Varela-Lopes, G. E., Molion, L. C. B.: Precipitation patterns in Cape Verde Islands: Santiago Island case study, Atmos. Clim. Sci., 4, 854–865, https://doi.org/10.4236/acs.2014.45075, 2014.

Vinatier, V., Wirgot, N., Joly, M., Sancelme, M., Abrantes, M., Deguillaume, L., and Delort, A. M.: Sidreophore in cloud waters and potential impact on atmospheric chemistry: Production by microorganisms isolated at the Puy de Dôme station, Environ. Sci. Technol., 50, 9315–9323, https://doi.org/10.1021/acs.est.6b02335, 2016.

Wedepohl, K. H.: The composition of the continental crust.: Geochim. Cosmochim. Acta, 59, 1217–1232, https://doi.org/10.1016/0016-7037(95)00038-2, 1995.

Willey, J. D., Kieber, R. J., Seation, P. J., Miller, C.: Rainwater as a source of Fe(II)-stabilizing ligands to seawater, Limnol. Oceanogr., 53, 1678–1684, https://doi.org/10.4319/lo.2008.53.4.1678, 2008.

Winton, V. H. L., Edwards, R., Bowie, A. R., Keywood, M., Williams, A. G., Chambers, S. D., Selleck, P. W., Desservettaz, M., Mallet, M. D., and Paton-Walsh, C.: Dry season aerosol iron solubility in tropical northern Australia, Atmos. Chem. Phys., 16, 12829–12848, https://doi.org/10.5194/acp-16-12829-2016, 2016.

Wu, H. Y., Hsieh, C. C., Ho, T. Y.: Trace metal dissolution kinetics of East Asian size-fractionated aerosols in seawater: The effect of a model siderophore, Mar. Chem., 254, 104277, https://doi.org/10.1016/j.marchem.2023.104277, 2023.

Yang, Y., Weber, R. J.: Ultrafiltration to characterize $PM_{2.5}$ water-soluble iron and its sources in an urban environment, Atmos. Environ., 286, 119246, https://doi.org/10.1016/j.atmosenv.2022.119246, 2022.

Yoon, J. E., Son, S., Kim, I. N.: Capture of decline in spring phytoplankton biomass derived from COVID-19 lockdown effect in the Yellow Sea offshore waters, Mar. Pollut. Bull., 174, 113175, https://doi.org/10.1016/j.marpolbul.2021.113175, 2022.

Yu, H., Tan, Q., Chin, M., Remer, L. A., Kahn, R. A., Bian, H., Kim, D., Zhang, Z., Yuan, T., Omar, A. H., Winker, D. M., Levy, R., Kalashnikova, O., Crepeau, L., Capelle, V., and Chedin, A.: Estimates of African dust deposition along the trans-Atlantic transit using the decadelong record of aerosol measurements from CALIOP, MODIS, MISR, and IASI, J. Geophys. Res. Atmos., 124, 7975–7996, https://doi.org/10.1029/2019JD030574, 2019.

Zhang, H., Li, R., Huang, C., Li, X., Dong, S., Wang, F., Li, T., Chen, Y., Zhang, G., Ren, Y., Chen, Q., Huang, R. J., Chen, S., Wang, X., Tang, M.: Seasonal variation of aerosol iron solubility in coarse and fine particles at an inland city in northwestern China, Atmos. Chem. Phys., 23, 3543–3559, https://doi.org/10.5194/acp-23-3543-2023, 2023.

Zhang, J., Zhou, X., Wang, Z., Yang, L., Wang, J., Wang, W. Trace elements in $PM_{2.5}$ in Shandong Province: Source identification and health risk assessment.: Sci. Total Environ., 621, 558–577, https://doi.org/10.1016/j.scitotenv.2017.11.292, 2018.

Zheng, G., Su, H., Wang, S., Andreae, M. O., Pöschl, U., Cheng, Y.: Multiphase buffer theory explains contrasts in atmospheric aerosol acidity, Science, 369, 1374–1377, https://doi.org/10.1126/science.aba3719, 2020.

Zhu, Q., Liu, Y., Shao, T., Tang, Y.: Transport of Asian aerosols to the Pacific Ocean, Atmos. Res., 234, 104735, https://doi.org/10.1016/j.atmosres.2019.104735, 2020.

Zhu, Y., Li, W., Wang, Y., Zhang, J., Liu, L., Xu, L., Xu, J., Shi, J., Shao, L., Fu, P., Zhang, D., and Shi, Z.: Sources and processes of iron aerosols in a megacity in Eastern China, Atmos. Chem. Phys., 22, 2191–2202, https://doi.org/10.5194/acp-22-2191-2022, 2022.